CHAPTER H

New Means of Shear Connection in Composite Steel-Concrete Joists – Drilled Standoff Screws

J.R. Ubejd Mujagic [1], W.S. Easterling[2], and T.M. Murray[3]

to be submitted to the ASCE Journal of Structural Engineering

ABSTRACT: Composite steel-concrete flexural members have become increasingly popular in design and construction of floor systems, structural frames, and bridges. A particularly popular system features composite trusses (joists) that can span large lengths and provide open web space for installation of typical utility conduits. One of the prominent problems with respect to composite joists has been the installation of welded shear stud connection due to demanding welding requirements and need for presence of the bulky welding equipment at the job site. This paper presents research results for a new type of shear connector developed at Virginia Tech – standoff screw. This type of connector is drilled, rather then welded, and represents a viable alternative to headed shear studs in composite joists. Results of experimental and analytical research are presented, as well as the development of a recommended design methodology. A numerical example is provided to illustrate the application of the design procedure.

CE Database keywords: composite joists, shear connectors, finite element analysis of shear connectors, steel-concrete composites, standoff screws, reliability, ductility of shear connectors.

H.1 BACKGROUND

Composite steel-concrete flexural members have become increasingly popular in design and construction of floor systems, structural frames, and bridges. While used in some form throughout most of the past century, especially in bridge construction, the use of such members has dramatically increased since the 1970s due to the introduction of formed steel

[1]Structural Engineer, Pinnacle Structures, Inc., Cabot, AR, [2]Professor, Via Department of Civil and Environmental Engineering, Virginia Polytechnic Institute and State University, Blacksburg, VA, [3]Montague-Betts Professor of Structural Steel Design, Via Department of Civil and Environmental Engineering, Blacksburg, VA

deck and concurrent advances in the field gained from experimental and analytical research. Research advances have in particular become apparent through the development of composite truss (joist) systems in the last 15 years. This type of system is economical and practical, as it results in decreased floor weight while allowing for wide range of spans and open web space for the installation of utilities. Traditionally, the most prominent drawback to this type of system has been shear connection. Specifically, due to relatively thin joist top chords, it is often difficult to satisfy the minimum base material thickness requirements for welding. Further, the need for significant welding equipment on the jobsite can be cumbersome, as well as deterrent for smaller projects.

In response to this problem, a new type of shear connector and associated design procedure were developed at Virginia Tech. Out of several types of such shear connectors considered, Hankins et al. (1994) determined that ELCO Grade 8 standoff screws, as illustrated in Fig. H.1, held the most promise for this application, and they were the subject of further research. Grade 8 refers to SAE Specification J429, which is equivalent to ASTM Specification A490 for Extra High-Strength Bolts. Concurrent and subsequent studies on this type of shear connector were conducted by Lauer et al. (1996), Alander et al. (1998), Webler et al. (2000), Mujagic et al. (2001), and Mason (2002). This paper presents a brief summary of experimental research previously reported by these authors. Additionally, the results of an extensive finite element study, the development of a strength prediction model and associated design procedure, reliability requirements, and recommendations are presented.

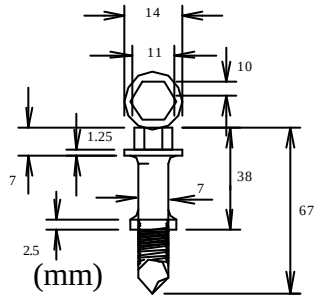

Figure H.1 Typical ELCO Grade 8 Standoff Screw

H.2 EXPERIMENTAL FINDINGS

Standoff screws were evaluated through three different types of tests. The first were pure shear and tensile tests. These were reported in detail by Mujagic et al. (2001). Because

they are easier to establish, the tensile strengths were used in the analysis. As determined through the tests, shear strength can be related to tensile strength by a coefficient of 0.6. Results of tensile tests did not vary significantly between various screw heights, and average recorded tensile strength of the screws, $F_{ut,sc}$, was 1207 MPa. The nominal tensile strength of ELCO Grade 8 screws is 1034 MPa.

Second, standoff screws were evaluated using push-out tests, which are a common and economical mean for assessing the strength of shear connection. The push-out specimens consisted of two 91.4 x 91.4 cm slabs connected to base steel sections using standoff screws. The steel section simulates a typical open web steel joist top chord constructed with double angles. Specimen fabrication and test procedures did not differ significantly between the studies referenced in the introduction. Specimen configuration included variations in slab construction (solid concrete slab or composite deck slab), slab thickness, deck depth, base material thickness, concrete strength, number of screws per specimen, and screw height above deck. Detailed descriptions of specimen fabrication, instrumentation and test set-ups for each specific series were reported by Mason et al. (2002).

A schematic of the typical push-out test configuration is shown in Fig. H.2. The push-out specimens were subjected to a vertical load that simulated the load at the steel concrete interface. Elastomeric bearing pads were placed under each slab to insure that the slabs were uniformly loaded along their bottom surfaces. The swivel and the loading plates, which were placed atop the steel section insured that the load from the hydraulic ram was evenly distributed between the two halves of the specimen and that the axial load indeed remained axial. A normal load distribution frame was used to simulate the application of gravity load in a composite joist and to prevent premature separation of the concrete and steel. The apparatus consisted of a hydraulic ram and two beams that were used to distribute normal load along the length of top chords.

The three quantities measured during the test were axial load, normal load, and slab vs. top chord relative slip. The axial load was measured with a load cell placed between the hydraulic ram and crosshead, as shown in Fig. H.2. Normal load was measured with a load cell that was placed between the normal load distribution frame and the hydraulic ram. Slip between the steel and composite slab were measured using linear potentiometers at four evenly distributed locations on each slab.

The loading scheme for all the tests was relatively similar. Axial load was applied in increments of 22-45 kN with normal load kept at 10% of the applied axial load. After each loading application, the system was left to stabilize for about three minutes, at which point all the measurements were recorded, and the next higher load was applied. Results of the tests are presented in Appendix I.

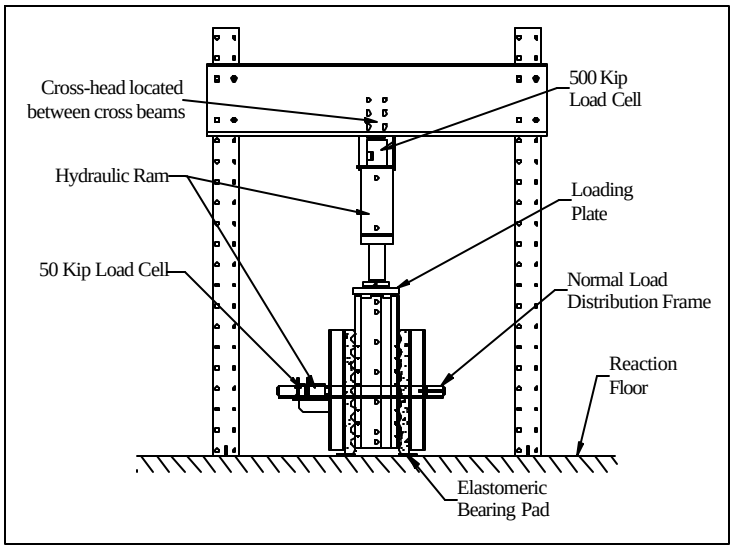

Fig. H.2 Push-Out Test Configuration (Alander et al. 1998a)

Six full scale composite joist tests were also conducted. These featured either one or two joists, member lengths between 7.3 and 12.2 m, and joist depths between 200 and 500 mm. All the details pertaining to fabrication and instrumentation of the specimens are described in detail by Lauer et al. (1996), and Mujagic et al. (2000). A schematic drawing of a typical test is shown in Fig. H.3, and the test parameters and results are summarized in Tables H.1 and H.2.

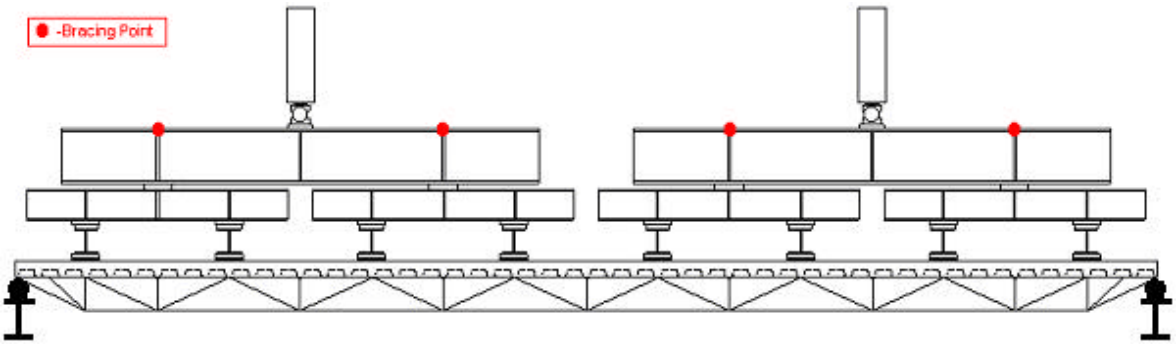

Fig. H.3 Full-Scale Test Configuration (Mujagic et al. 2000b)

Table H.1 Full-Scale Test Geometric Parameters

Test	L (m)	d (mm)	t_s (mm)	Deck Type	w_{r1} (mm)	w_{r2} (mm)	TOP CHORD	BOTTOM CHORD	h_r (mm)	H_s (mm)	N	l_s (mm)
CSJ-8	9.02	457	102	1.0C	23	70	2L-38.1x38.1x3.1	2L-50.8x50.8x4.1	25	51	1*	92
CSJ-9	9.02	457	89	1.0C	23	70	2L-38.1x38.1x3.1	2L-50.8x50.8x4.1	25	51	1*	92
CSJ-10	6.10	203	64	0.6C	19	44	2L-25.4x25.4x2.8	2L-31.8x31.8x3.4	14	51	1*	86
CSJ-11	12.2	508	102	1.5VL	44	64	2L-50.8x50.8x6.4	2L-88.9x88.9x7.3	38	64	1*	81
CSJ-12	9.14	508	89	1.0C	23	70	2L-38.1x38.1x3.5	2L-44.5x44.5x4.3	25	64	1	104
CSJ-13	12.2	508	127	2VL	127	178	2L-76.2x76.2x8.0	2L-102x102x11.1	51	102	4	216

Table H.2 Full-Scale Test Results

Test	f'_c (MPa)	$F_{y,tc}$ (MPa)	$F_{u,tc}$ (MPa)	$F_{y,bc}$ (MPa)	M_{ta} (kN-m)	M_a (kN-m)	ΣQ_{ta} (kN)	Q_{ta} (kN)	Reported Failure
CSJ-8	24.8	385	580	409	141.9	119.4	143.7	16.0	Top Chord Buckling
CSJ-9	31.7	385	588	452	185.6	164.0	246	13.7	Bottom Chord Fracture
CSJ-10	34.5	442	603	462	50.9	46.5	234.4	12.3	Top Chord Yielding
CSJ-11	31.7	387	574	415	520.3	441.6	624.5	17.3	Shear Connection Failure
CSJ-12	35.2	403	556	419	180.4	158.6	312	20.8	Bottom Chord Yielding
CSJ-13	26.2	352	533	412	860.8	763.1	1297.5	17.1	Screw Shear

*Estimated.

where:

L = joist length (m)
d = joist depth (mm)
t_s = slab thickness (mm)
w_{r1} = bottom rib width (mm)
w_{r2} = top rib width (mm)
h_r = rib height (mm)
l_s = length of failure plane, mm
f'_c = concrete compressive strength (MPa)
$F_{y,tc}$ = top chord yield strength (MPa)
$F_{y,bc}$ = bottom chord yield strength (MPa)
M_{ta} = total load moment (kN-m)
M_a = applied load moment (kN-m)
ΣQ_{ta} = horizontal shear at M_{ta} (kN)
Q_{ta} = horizontal shear/screw at M_{ta} (kN)

H.3 FINITE ELEMENT ANALYSIS

Finite element analysis (FEA) was used as a complementary tool in the analysis of the experimental data. It was important in determining the influence of variables that were not evaluated through testing, such as influence of screw diameter or strength parameters of base angle. Further, it was useful in providing the theoretical basis for relationships established through the analysis of test results. FEA was accomplished using ABAQUS Standard v.6.3 (HKS 2003).

H.3.1 Material Properties used in FEA

To successfully model the strength and behavior of shear connection using the finite element method, it was first necessary to define the mechanical properties of the base steel, slab concrete, and shear connector steel. Material constitutive models were simplified to facilitate a more efficient analysis, but were kept sufficiently detailed to capture the important features of the material response.

H.3.1.1 Properties of Concrete

The stress-strain response for concrete in compression, as illustrated in Fig. H.4, is modeled as a simplified bilinear relationship. The value of ε_{cy} is taken as $f_c^{'}/E_c$, and the value of ε_{cu} is taken as 0.0038. The concrete modulus of elasticity is given in Eq. H.1 (ACI 2002).

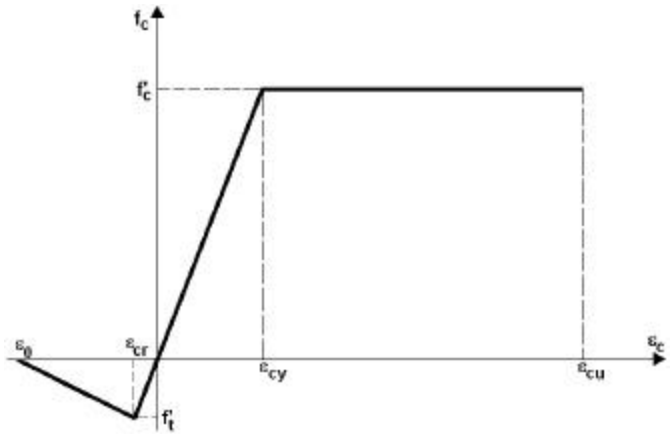

Fig. H.4 Concrete Stress-Strain Model

$$E_c = 0.043 w_c^{1.5} \sqrt{f_c^{'}} \qquad \text{(Eq.H.1)}$$

where:

E_c = concrete modulus of elasticity, MPa

w_c = concrete unit weight, kg/m^3

f'_c = concrete compressive strength, MPa

The tensile strength, $f_t^{'}$, was taken as $(0.75)\sqrt{f_c^{'}}$ per Carreira and Chu (1986), and corresponding strain, ε_{cr}, was taken as $f_t^{'}/E_c$. According to Lin and Scordelis (1975), $\varepsilon_0 = 10\varepsilon_{cr}$. In the absence of reinforcement in the tensile zone around the shear connector, the stress-strain approach causes unreasonable mesh sensitivity (HKS 2001b). For this reason, the concrete response in tension was modeled using fracture energy principles proposed by Hilleborg et al. (1976). The fracture energy required to open a unit area crack, G_f, is defined by Eq. H.2.

$$G_f = \int f_t du \qquad \text{(H.2)}$$

The assumed response is shown in Fig. H.5. The displacement, u_0, approximately corresponding to strain ε_0, is taken as 0.065 mm in the analysis. Concrete strengths used were in the range between 17.2 and 51.7 N/mm^2.

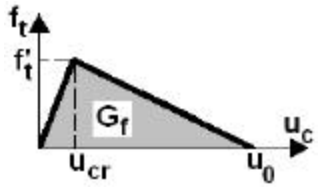

Fig. H.5 Fracture Energy Cracking Response of Concrete

H.3.1.2 Properties of Steel: Angle Material and Standoff Screws

Simplified multi-linear stress-strain curves based on those provided by Salmon et al. (1996) were used to model the response of A36M (F_y = 345 MPa) and A572M Gr. 345 structural steels, used for base angle/flange material. The response is the same in compression and tension. Nominal stress-strain properties are given by Fig. H.6 and Table H.3. Additional stress-strain curves were obtained by offsetting the inelastic curve parts vertically in desired stress increments. A36M steels were investigated in the range in between 207 and 345 MPa. This range for A572M steels was in between 276 and 552 MPa.

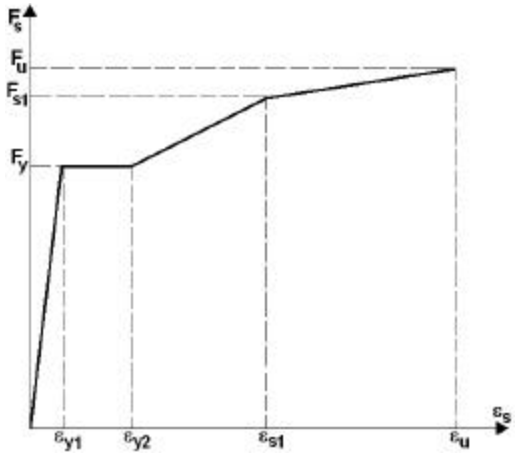

Fig. H.6 Structural Steel Stress-Strain Curve

Table H.3a Steel Curve Stress Values

STRESS	A36M GR.250	A572M GR. 345
F_y	250 (36)*	345 (50)*
F_{s1}	351 (50.91)*	451 (65.45)*
F_u	405 (58)*	483 (70)*

*MPa (ksi)

Table H.3b Steel Curve Strain Values

STRAIN	A36M GR.250	A572M GR. 345
e_{y1}	0.00124	0.00172
e_{y2}	0.01405	0.02100
e_{s1}	0.10000	0.10000
e_u	0.20000	0.18000

Standoff screw material is specified by the requirements of SAE J429 Gr. 1034 material. The nominal stress-strain response used in modeling is given by Fig. H.7 and Table H.4 in the form of a simplified tri-linear curve. Additional stress-strain curves were

generated using the same method as for the structural steel. The range of $F_{ut,sc}$ investigated in this study was between 965 and 1310 MPa.

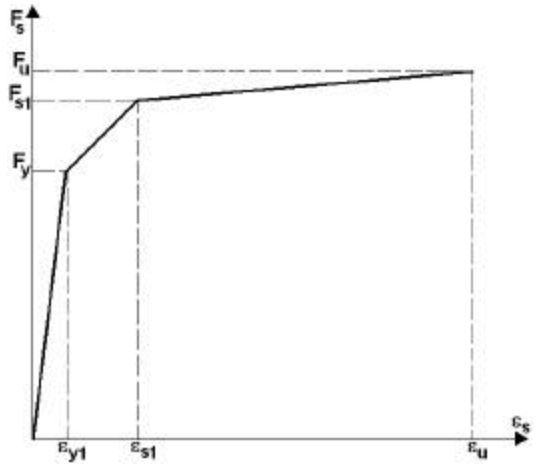

Fig. H.7 Standoff Screw Stress-Strain Curve

Table H.4 Stress-Strain Curve for Screws

STRESS	STRAIN	STRESS
e_y, F_y	0.00368	735 (106.61)*
e_{s1}, F_{s1}	0.01061	984 (142.78)*
e_u, F_u	0.07738	1034 (150)*

*MPa (ksi)

For analytical purposes, the above given engineering stress and strain properties for the steels were converted to true stress and logarithmic plastic strain using Eqs. H.2 and H.3 (HKS 2001a).

$$f_{true} = f_{eng}(1+\varepsilon_{eng}) \tag{H.2}$$

$$\varepsilon_{ln}^{pl} = \ln(1+\varepsilon_{eng}) - f_{true}/E \tag{H.3}$$

H.3.2 Method of Analysis

Finite element models used to investigate screw shear (both in solid and ribbed slabs), and concrete rib failures consisted of three-dimensional solid elements. The size of models varied according to the needs of parametric studies, however, most models were built to approximately resemble the configuration and loading of push-out tests, as illustrated in Fig. H.8. The slab was modeled as a 900 x 900 mm element, fixed against displacements and rotations from all sides except the bottom (i.e., side adjacent to the angle). The joist angles, or top chords, were modeled as flat plates, free to displace in the direction of the load, but fixed against displacement and rotation on the interior side representing plate thickness. The geometry of standoff screws was simplified for the purpose of this modeling, as illustrated in in Fig. H.9. Specifically, the standoff screw shank washer was eliminated, and the screw head was solidified. The features eliminated with these simplifications are not important to the behavior of the screw, but rather its installation.

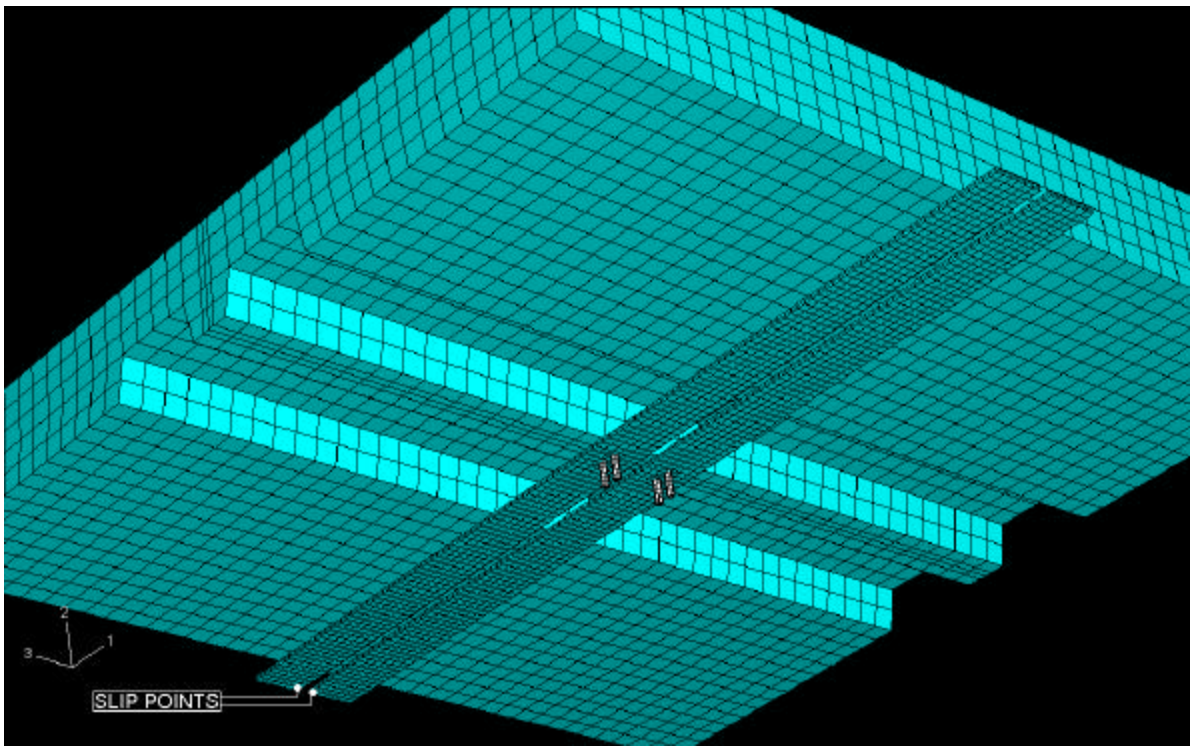

Fig. H.8a Finite Element Models: Mesh Structure

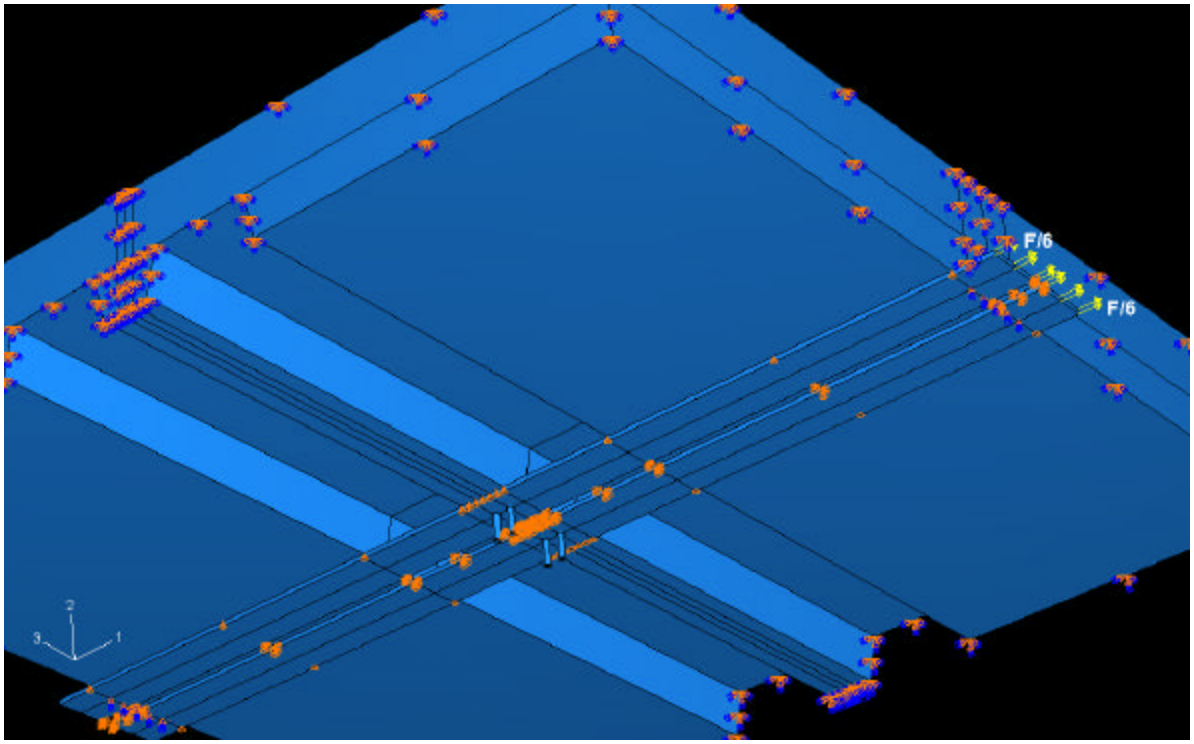

Fig. H.8b Finite Element Models: Loading and Boundary Conditions

The front surface of the standoff screws (i.e. bearing surface of the screw) was attached to slab using the ABAQUS embedded element feature. This technique recognizes that there is a separation between the concrete and the back of the screw at a fairly early loading stage. The same observation was mad by Jayas and Hosain (1987) with respect to behavior of headed shear studs. El-Lobody and Lam (2002) employed a similar technique while modeling headed shear studs in composite steel–hollow concrete members. With the embedded element feature, the need to model an opening in the embedding element is eliminated, and the software automatically ties the most adjacent nodes between the embedding and the embedded elements, based on coordinates of the two provided by the user. The drawback of the embedded element feature is that in the analysis it considers the embedded element to be subject to translation only and not rotation. This was compensated for in the analysis by un-embedding a certain length of the screw adjacent to the top chord (Fig. H.9). Further, this un-embedment length was found to be effective in compensating for the inability of the concrete fracture model to adequately account for physical displacements in damaged concrete. Early pre-failure damage in the concrete is evident in the region between the shank base and top chord. Such damage has an effect on screw slip, although it does not have significant impact on strength. Standoff screws were attached to the top chord via ABAQUS analytical tie feature, where the nodes on the top chord holes are attached to the most closely positioned nodes on the screw. Finally, the analysis was performed assuming no-frictional sliding of top chord with respect to the slab. It was found through the comparison of test data and numerical models that an optimum length of un-embedment is 7.6 mm for ribbed slabs and 2.5 mm for solid slabs. Comparisons of representative test results and equivalent FE models are shown in Figs. H.10 through H.12.

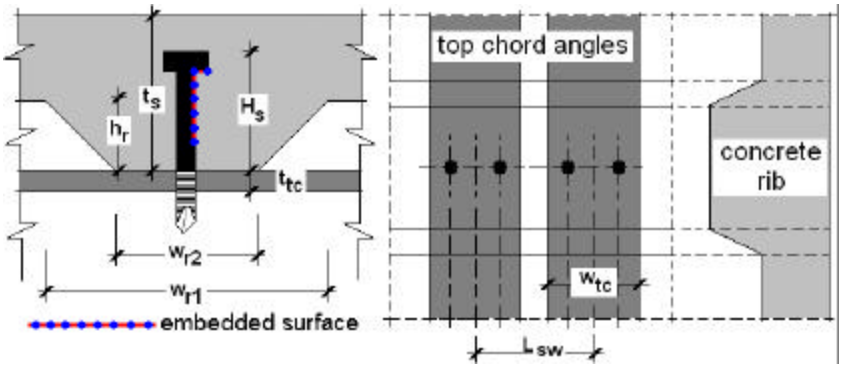

Fig. H.9 FEM Modeling Parameters and Screw Embedment

Modeling of screw pullout failures proved to be quite difficult. Namely, both strength and slip are heavily dependant on the interaction between screw threads and threads along the surface of the angle hole. While the grip on the screw is not complete, some interaction between screws threads and the base angle exists on the non-bearing screw surface, and failures occurs when at least a part of the top chord hole tears enough to allow the screw to slip out. Further, to adequately represent the actual condition, it is necessary to model the connection slip that results from the deformation of the concrete. It was determined that both the connection capacity, and the corresponding slip can be predicted using FE models if the failure is defined as the point at which one half of the nodes around the top chord hole upper surface reach the material rupture stress, $F_{u,tc}$. Additionally, the configurations of FE models used for other types of failure needed two adjustments. First, the concrete was modeled as elastic-perfectly plastic material with stress-strain properties identical with the compression curve of Fig. H.4. And secondly, slab cavity equal to the shape of the screw shank was created. The screw shank was attached to this cavity using the ABAQUS analytical tie feature. Other modeling aspects were similar to those used for other types of failures. Details of the FEA performed in this study are given by Mujagic and Easterling (2003).

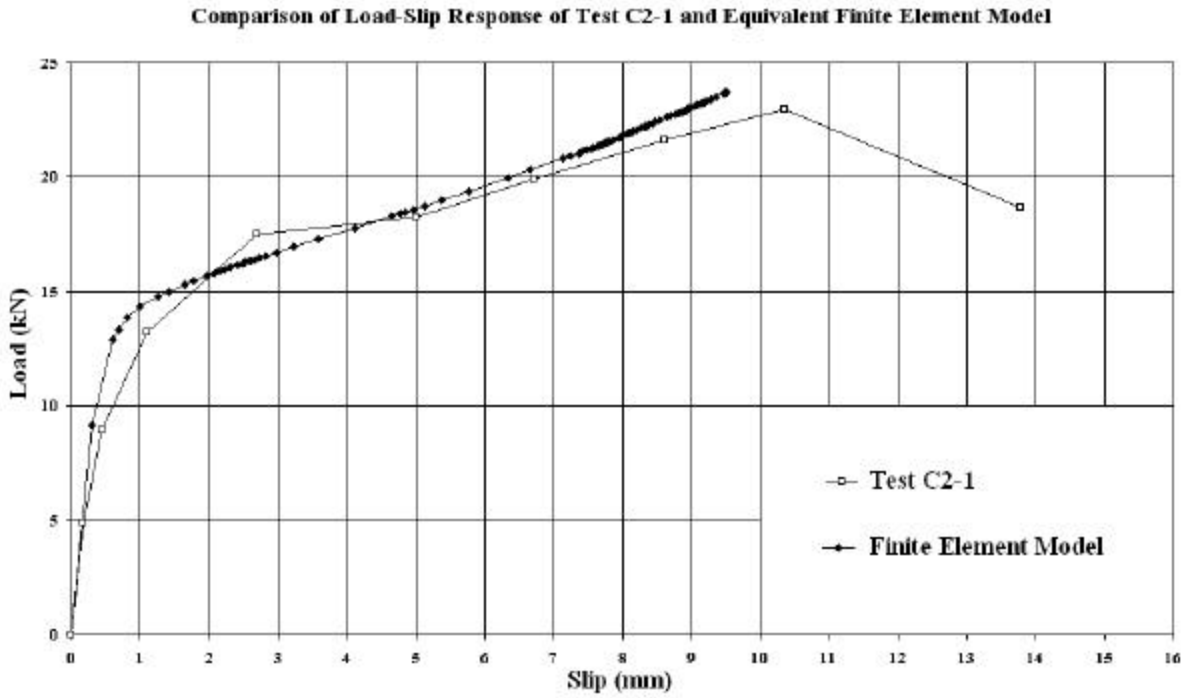

Fig. H.10 Comparison of Experimental and Numerical Model of Screw Shear Failure

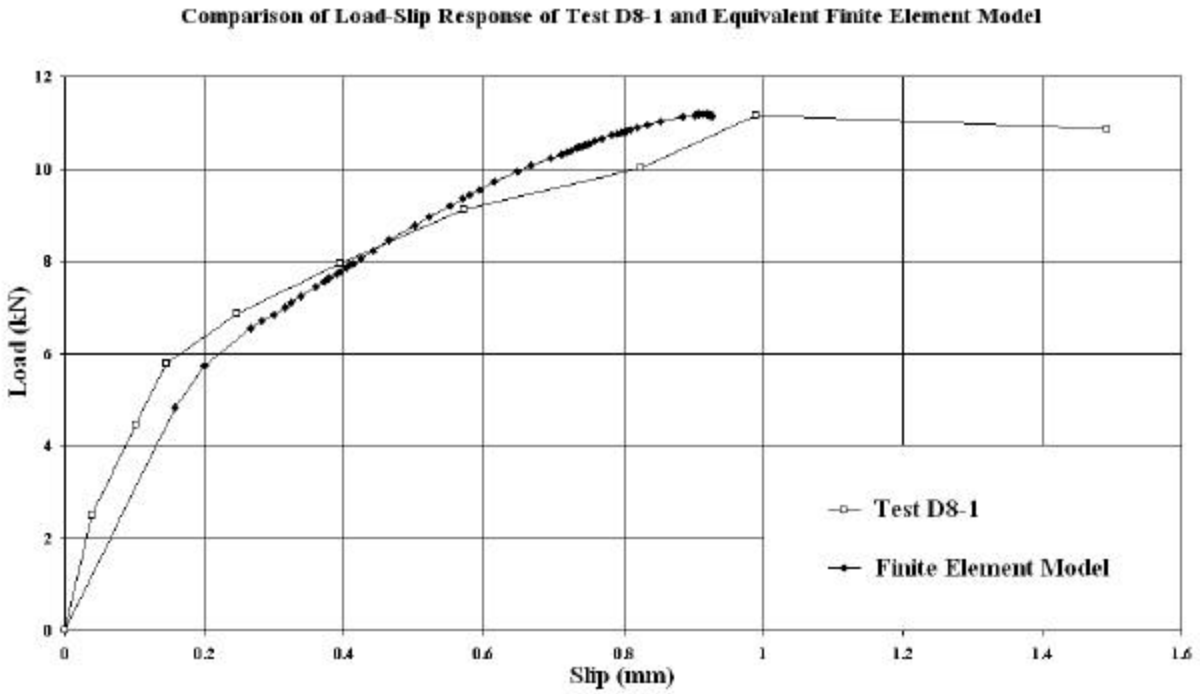

Fig. H.11 Comparison of Experimental and Numerical Model of Brittle Concrete Failure

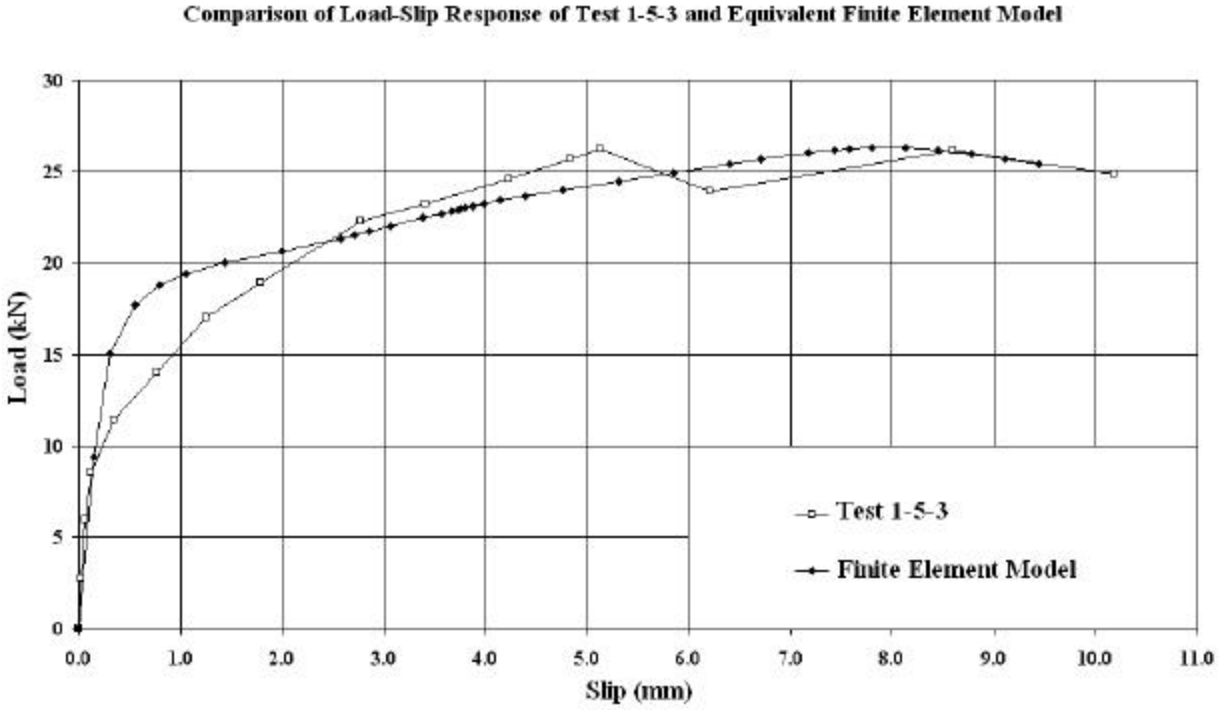

Fig. H.12 Comparison of Experimental and Numerical Model of Solid Slab Failure

H.4 STRENGTH PREDICTION MODEL

In deriving the strength prediction model, the goal was to build on previously developed concepts reported by Mujagic et al. (2001), and expand the scope of the existing strength prediction models. Also, the intent was to develop dimensionally correct, yet simple, formulae, which are easy to codify and adapt in other similar applications. The resulting strength prediction model consists of three distinct limit state equations. Each of them predicts the strength for one of the three applicable modes of failure (i.e, screw shear, concrete rib failure and screw pull-out). The strength of a particular shear connector configuration is then established as the strength computed with the governing limit state equation.

H.4.1. Screw Shear

Screw shear is a limit state in which a standoff screw fractures through its threaded part, while damage to the slab and top chord is relatively small. Such failures were observed both in solid slab and ribbed slab specimens. As determined earlier (Mujagic et al. 2001), the strength of standoff screw connectors in solid slabs, and ribbed slabs when ribs are parallel to the joist, can be adequately represented by the screw strength in simple shear (Eq. H.4). As anticipated, FEA shows that the strength is directly proportional to the screw cross-sectional area. In tested solid-slab specimens, only screw shear failures were seen. The same observation was made in the FEA. Namely, even with D_e = 12.7 mm and f'_c = 17.2 MPa, the modeled specimens still failed by screw shear. Therefore, it can be concluded that screw shear is the only mode of failure applicable to solid slabs and the ribbed slabs with ribs parallel to the joist. Equation H.4 is associated with a coefficient of variation (C.O.V.) of 11% and a mean ratio of tested to predicted strength of 1.08.

$$Q_n = 0.6 A_e F_{ut,sc} \qquad \text{(Eq. H.4)}$$

where:

Q_n = nominal screw strength, N

A_e = area based on D_e, mm

D_e = effective stress diameter, mm

$= D - 24.75/n$ (UNF)

n = number of threads per inch

$F_{ut,sc}$ = screw tensile strength stress, MPa

The FEA results support the conclusion that the screw shear strength in slabs with formed deck with ribs perpendicular to the joist is significantly affected by top chord thickness. The same observation was made based on experimental data (Mujagic et al. 2001). Specifically, with the deforming top chords, screws tend to rotate, as illustrated in Fig. H.13. As a result, the threaded failure plane is loaded in both shear and tension. The screw rotation tends to increase with thinner top chords. Therefore, unless other conditions result in a screw pull-out, thinner top chords will typically result in higher strengths per screw.

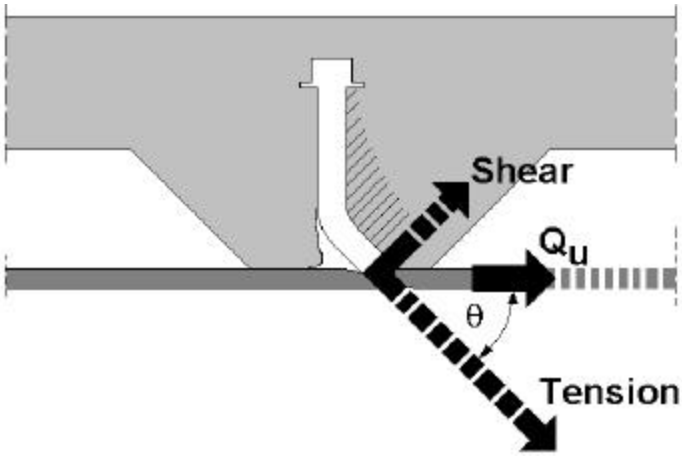

Fig. H.13 Connector Rotation in Screw Shear Failures

The FEA leads to a conclusion that top chord width also plays a significant role in screw shear based strengths. The effect is approximately opposite to that of thickness. The effect of top chord thickness (left) and top chord width (right) on strength generated by FEA parametric study is illustrated in Fig. H.14.

To account for screw rotation, a non-dimensional top chord adjustment coefficient, C_{tc}, was derived. This coefficient, as given by Eq. H.5, was derived by applying the trends observed in the FEA to experimental data, and then by making adjustments to achieve the best statistical fit. To calculate the screw shear based strengths in ribbed slabs, the strength calculated by Eq. H.4 should be multiplied by C_{tc}. The resulting model yields a mean ratio of tested to predicted strength of 1.02, and a C.O.V. of 14%.

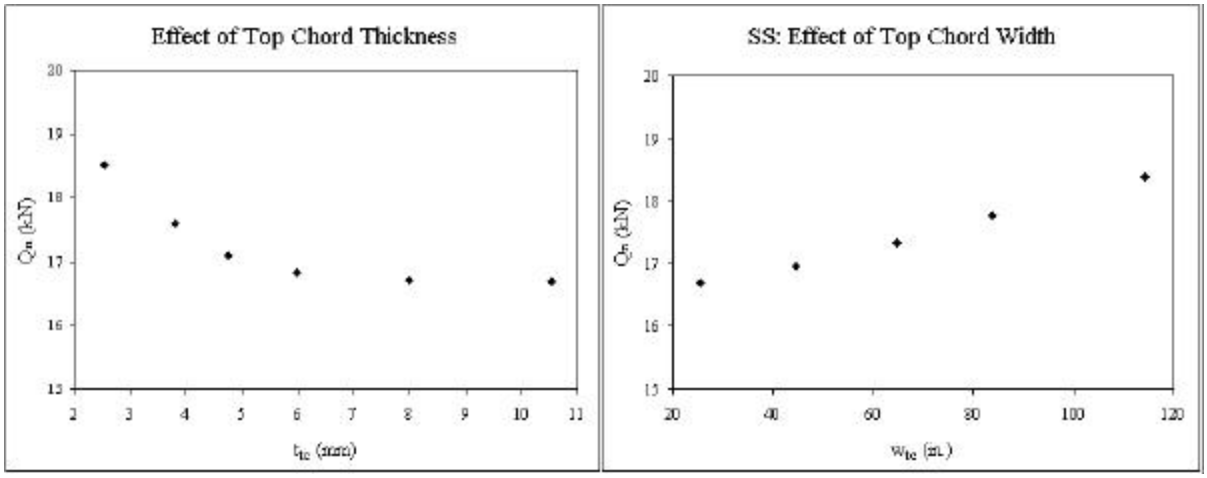

Fig. H.14 Effect of Top Chord on Screw Shear Failure

$$C_{tc} = \frac{1}{4}\sqrt{\frac{w_{tc}}{t_{tc}}} \leq 1.0 \qquad \text{(Eq. H.5)}$$

Other variables, such as w_{r1}, $F_{y,tc}$, and H_s were found to have minor impact on strength, and can safely be excluded from the strength prediction model.

H.4.2 Concrete Rib Failure

Concrete rib failure is a type of limit state in which a concrete cone is separated and pulled out of the slab by the embedded screw, or more often, the group of screws. With this type of failure, damage to screws and top chord is minimal. Concrete rib failure occurs along a failure plane whose length, L_{fp}, depends on screw height and rib geometry. This plane is depicted in Fig. H.15, and its general case is given by Eq. H.6. The term L_s in Eq. H.6 denotes the screw spacing in the direction of the joist, and is depicted as length b in Fig. H.15. The other variables in Eq. H.6 are defined by Fig. H.9. As can be seen from Fig. H.15, most of the length of this plane is subject to some combination of orthogonal forces resulting from horizontal shear. The stress condition resulting from these forces is difficult to describe analytically. A major source of this difficulty is the large statistical scatter typically found in applications involving concrete material, which makes it difficult to confirm a stipulated analytical solution through comparison with experimental data. The most practical solution was to develop an expression of an effective concrete stress, f_{ce}, that would be assumed to act over the entire surface of the failure plane and which would be expressed in terms of f_c'.

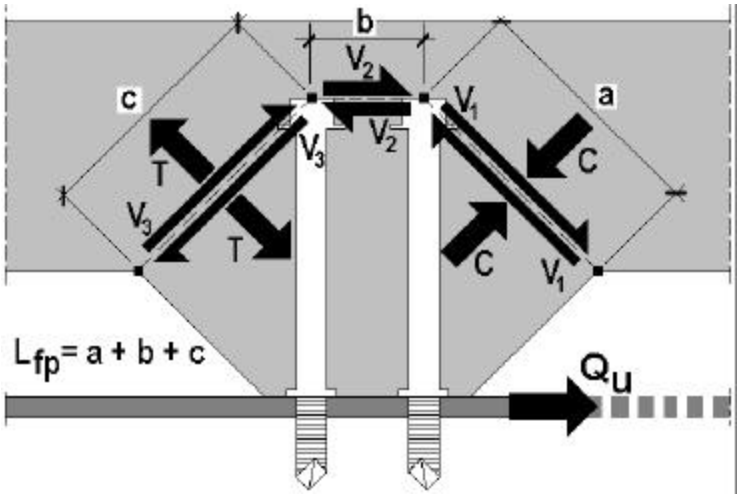

Fig. H.15 Failure Plane in Concrete Rib Failures

$$L_{fp} = L_s + 2\sqrt{\left(\frac{w_{r2} - L_s}{2}\right)^2 + (H_s - h_r)^2} \qquad \text{(Eq. H.6)}$$

Due to statistical variability inherent in concrete as structural material, observing the effect of f_c' on the concrete rib failure is quite difficult. An earlier study by Mujagic et al. (2001) considered several possible models to represent the influence of f_c' on concrete rib failure based strength. It was determined that $\ln(f_c')$ statistically best reflects the test results. However, a clear picture in this regard could not be gained due to high statistical scatter of data, mostly due to lack of predictability inherent in concrete.

The FEA performed in this study shows that both $\ln(f_c')$ and $\sqrt{f_c'}$ represent reasonably well the influence of concrete strength in concrete rib failures. The results of a FEA parametric study, which compares the same specimens with different values of f_c', are shown in Fig. H.16. As can be seen, $\sqrt{f_c'}$ adequately represents the influence of concrete strength, and f_{ce} can then be given as $\chi\sqrt{f_c'}$, where χ is a constant determined from statistical analysis of the experimental data.

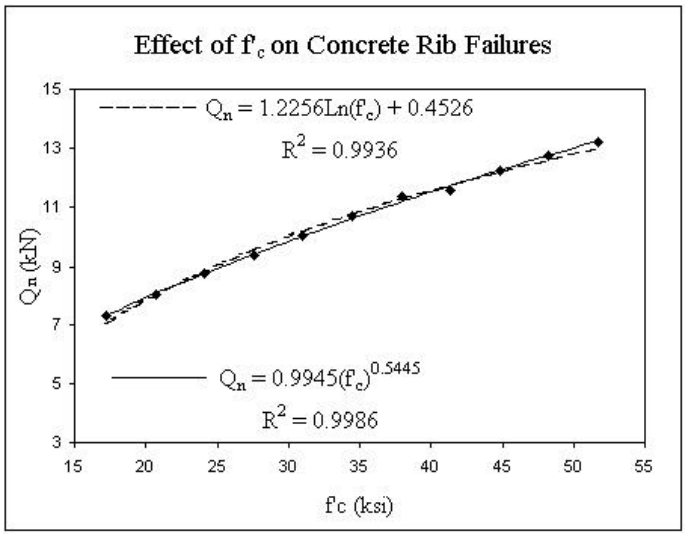

Fig. H.16 Effect of f'c on Concrete Rib Failure Based Strength

Next, it was necessary to determine the width of the failure stress surface. Both experimental data and FEA lead to the conclusion that the concrete rib failure based strength is unrelated to the screw spread along the rib length, L_{sw}. This length is illustrated in Fig. H.9 and is more accurately defined as the lateral distance between centroids of screw clusters in a rib. However, the FEA showed that the concrete rib failure based strength is proportional to the screw diameter, or more accurately, the screw cross-sectional area, as illustrated in Fig. H.17. While the effect of screw diameter cannot be evaluated through the existing experimental data, it is reasonable to conclude that the failure plane width is proportional to the screw diameter, based on FEA.

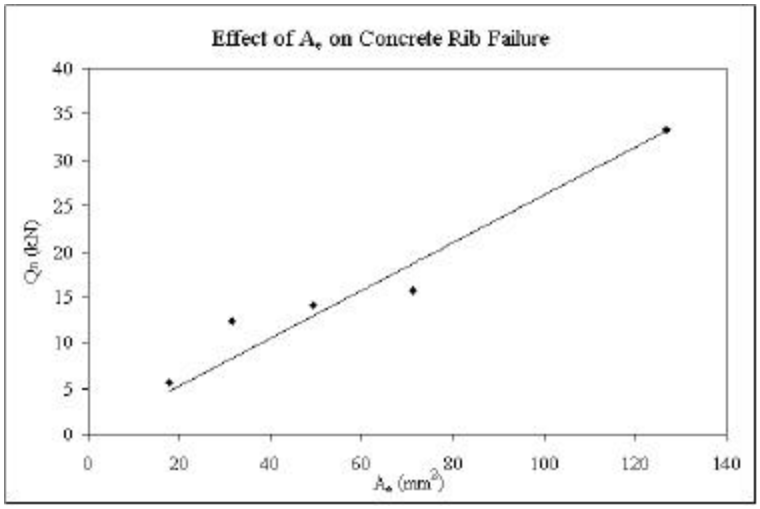

Fig. H.17 Effect of A_e on Concrete Rib Failure

Lastly, the number of screws per rib, N, was found to be a variable with a significant impact on concrete rib failure based strength. Specifically, each screw, or row of screws has its own tributary failure plane. If a higher number of screws per rib is used, and especially, if more screws are concentrated in a smaller area, the tributary failure planes will overlap, and as a result, a smaller strength per screw is obtained. The FEA does not offer a clear picture with respect to the influence of N on strength. The reason is lack of consistency in mesh arrangement in subsequent models, where additional screws are added. The influence of N was therefore evaluated solely using test results. From statistical analysis of data, it was found that $N^{2/3}$ best represents the influence of screw grouping, as illustrated in Fig. H.18. Having considered the effect of all major variables, the resulting strength prediction model is shown as Eq. H.7.

$$Q_n = \frac{8.75 f_{ce} D_e L_{fp}}{N^{2/3}} \qquad \text{(Eq. H.7)}$$

where:

f_{ce} = effective concrete stress, MPa

$= 0.75\sqrt{f_c'}$

Eq. H.7 gives a mean of 0.98 and C.O.V. of 17%. The influence of other variables can be neglected, as they result in no significant improvement in C.O.V.

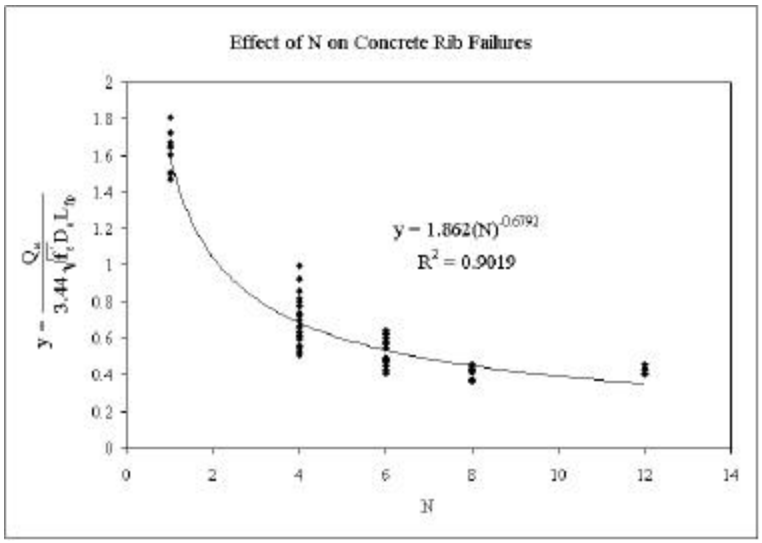

Fig. H.18 Influence of N on Concrete Rib Failure

H.4.3 Screw Pullout

Screw pullout is a limit state typical for configurations where standoff screws are drilled into relatively thin angles. The pullout occurs due to severe deformation of angle in the region of screw embedment (Fig. H.19a), where damage to both slab and screw is minimal, although significant rotation of screws is present (Fig. H.19b). The loading on the perimeter of the hole is a combination of bearing on the hole, commonly seen in structural bolted connections, and punching shear, commonly seen in rod brace anchorages in steel columns. The extent to which either former or the latter is represented depends on screw diameter, and top chord thickness.

While top chord tearing in a hole region where bearing occurs is a factor in screw pullout, both the experimental data and the FEA, as illustrated in Fig. H.20, show that the strength can be adequately described as a function $F_{y,tc}$ for A36M and A572M steels. Fig. H.20 shows the relationship between combined values of $F_{y,tc}$ for A36M and A572M steels and the screw pullout based strength. The practical benefit of this is that a designer can compute the screw pullout based strength without knowing the value of $F_{u,tc}$.

Another significant aspect of behavior is the relationship between the screw diameter and strength. As observed through FEA, and shown in Fig.H.21, the strength per screw increases with increasing screw diameter, as both the bearing width and the area of threaded grip increase. However, Fig. H.21 also shows that if screws of relatively large diameter are drilled into relatively narrow top chords, the pattern describing the effect of D_e strength suddenly changes. The reason is the severe deformation of top chord and apparent top chord failure in tension. This event can be viewed as particular to the numerical modeling, because it is not likely to occur in practical applications. Namely, configurations warranting larger screw diameters will also likely warrant larger top chord to satisfy the flexural strength requirements. As a practical matter, the ratio of top chord width to effective screw diameter, w_{tc}/D_e, should be no less than 4.0.

a. 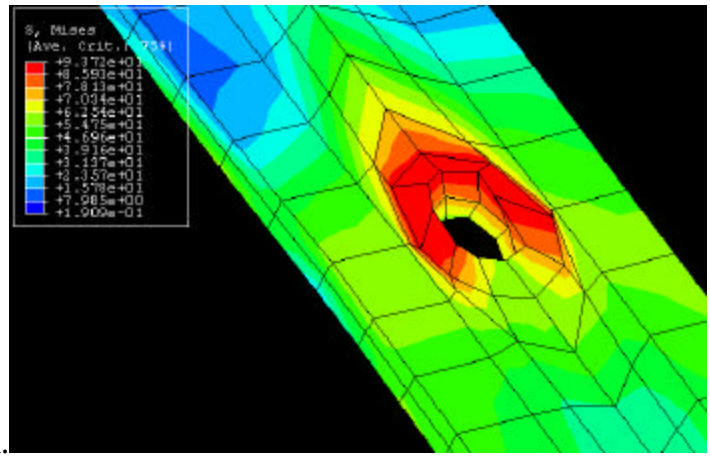 b. 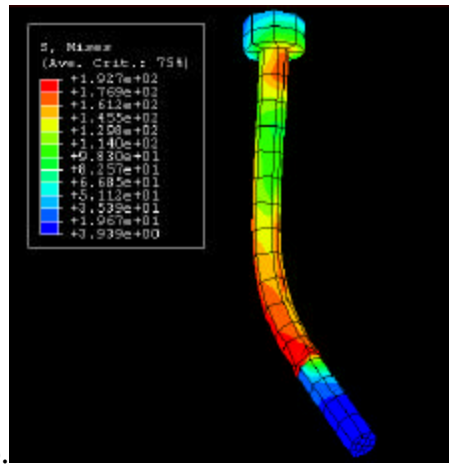

Fig. H.19 Post-Failure Deformations in Screw Pullout: (a.) Top Chord, (b.) Screw

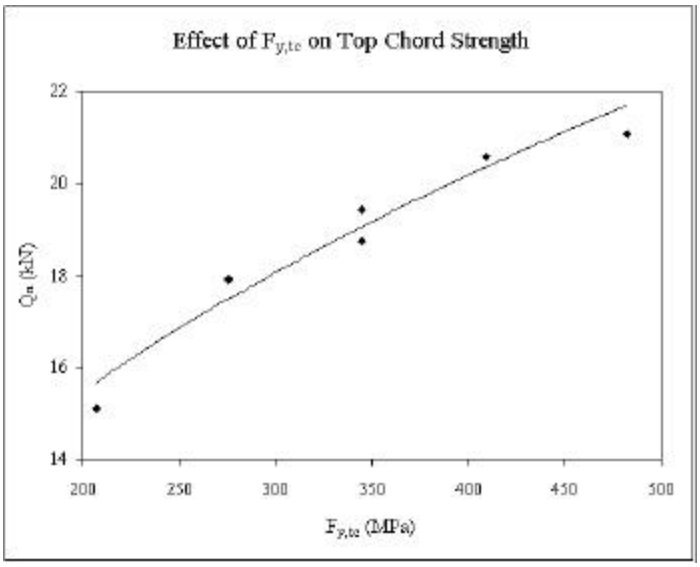

Fig. H.20 Effect of $F_{y,tc}$ on Screw Pullout Based Strength

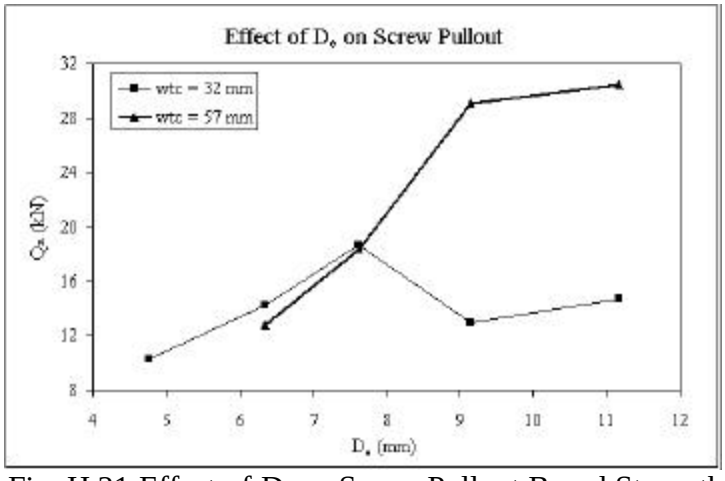

Fig. H.21 Effect of D_e on Screw Pullout Based Strength

Both FEA and the test results show a similar pattern by defining the effect of top chord thickness on strength. The strength gradually increases with an increasing top chord thickness. With the effect of all variables of significant impact combined, Eq. H.8 was developed. In comparison with the test data, it has a mean of 1.00 and C.O.V. of 9%. While other variables, such as H_s, h_r, and w_{tc} have some impact on strength, such impacts are minor and can be neglected without severe effect on C.O.V.

$$Q_n = \frac{(D_e)^{1.6}(t_{tc})^{0.4}\sqrt{E_s F_{y,tc}}}{17.2} \qquad \text{(Eq. H.8)}$$

where:

E_s = steel modulus of elasticity, MPa

H.4.4 Summary of the Strength Prediction Model

The complete model for prediction of strength of standoff screws is given by Eq. H.9. As noted earlier, w_{tc}/D_e should not be smaller than 4.0. Also, when solid slabs are encountered, or when slab ribs are oriented parallel to the joist, the second and third equations in the strength computation model are to be excluded. Further, the model is limited to A36M and A572M steels, the screw diameters between 4.8 and 12.7 mm, concrete compressive strengths between 17.2 and 51.7 MPa, and top chord thickness between 2.5 and 12.7 mm.

$$Q_n = \min\left\{0.6C_{tc}A_e F_{ut,sc};\quad \frac{(D_e)^{1.6}(t_{tc})^{0.4}\sqrt{E_s F_{y,tc}}}{17.2};\quad \frac{8.75 f_{ce} D_e L_{fp}}{N^{2/3}}\right\} \qquad \text{(Eq. H.9)}$$

where:

C_{tc} = top chord adjustment factor

$= \frac{1}{4}\sqrt{w_{tc}/t_{tc}} \le 1.0$, for slab ribs perpendicular to joist

= 1, for solid slabs and those with ribs parallel to joist

When compared to the experimental data consisting of 271 push-out tests, Eq. H.9 yields a mean of 1.03 and a C.O.V. of 15%. A diagram showing the distribution of tested to

predicted strength ratios is shown in Fig. H.22. Comparison of full-scale test theoretical and tested moment strength is provided in Table H.5. Computed values are based on the strength calculation model for standoff screws presented in Eq. H.9.

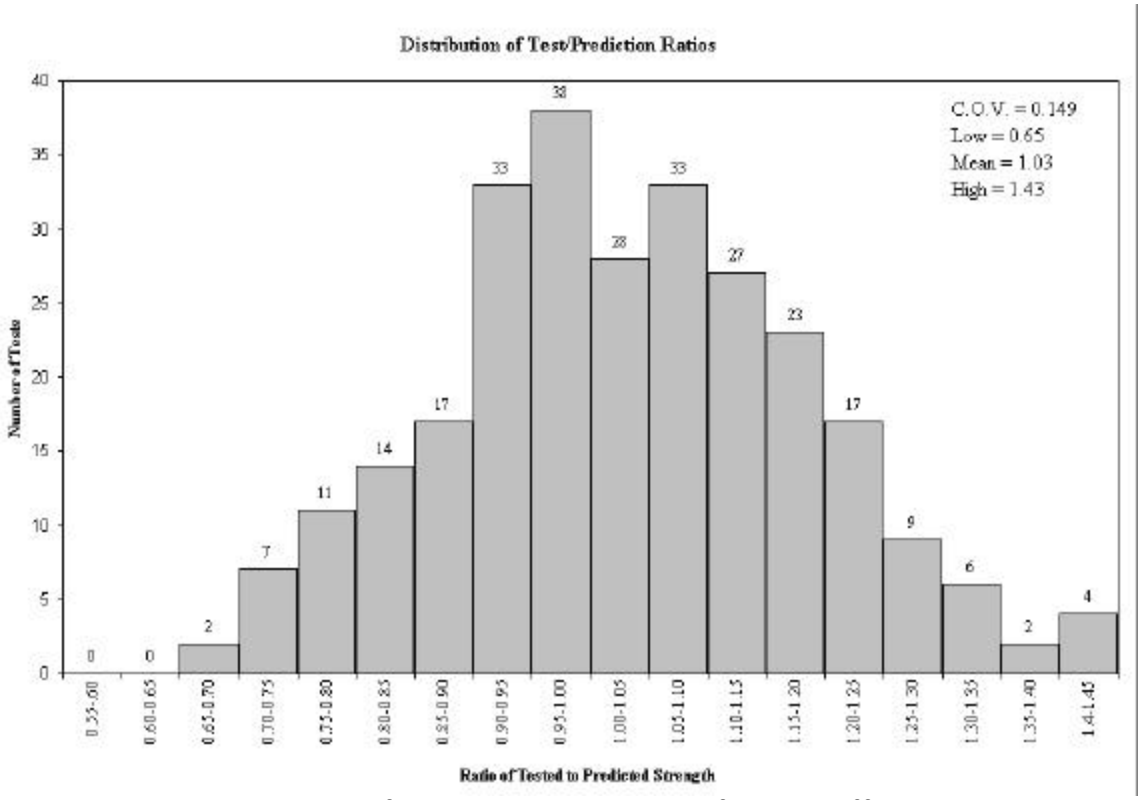

Fig. H.22 Distribution of (Test/Prediction) Ratios for Standoff Screw Model

H.5 DUCTILITY REQUIREMENTS

In favorable scenarios, there is enough slip capacity in connectors to allow for redistribution of longitudinal shear. This allows shear connectors along a span to carry equal loads. Joists are typically designed as fully composite with the limit state defined as yielding of the bottom chord. The slip distribution at the maximum load for CSJ-12, which failed by bottom chord yielding, is shown in Fig. H.23. It can be seen that slip is fairly uniform in the region in which the screws are spaced, suggesting that the redistribution of shear has occurred. In contrast, Fig. H.24 shows the similar plot for test CSJ-13. Although the specimen was designed as fully composite, based on the strength requirements of standoff screws, due to a lack of shear connector ductility the redistribution of longitudinal shear did not occur and shear connection failed prematurely, thus causing the failure of a premature failure of the joist as well.

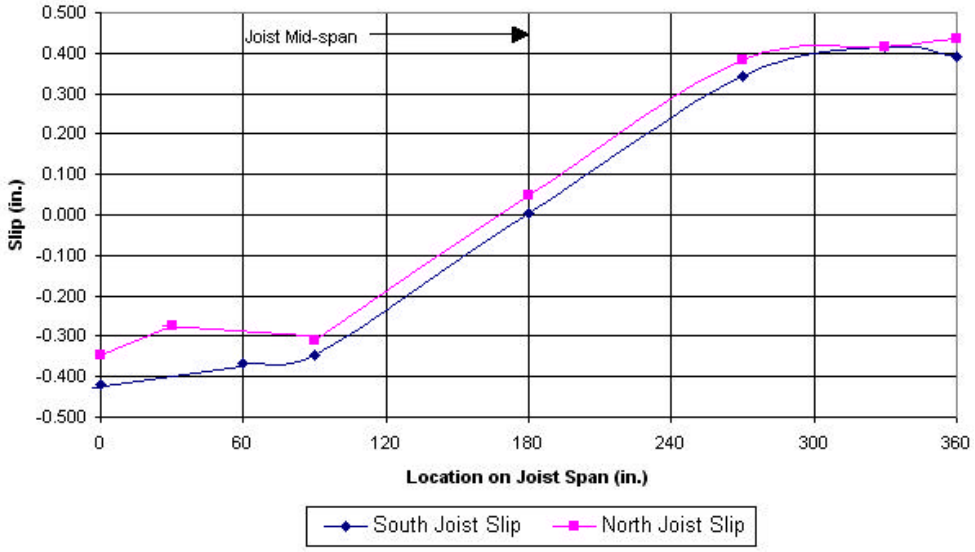

Fig. H.23 Test CSJ-12 Slip at Maximum Load

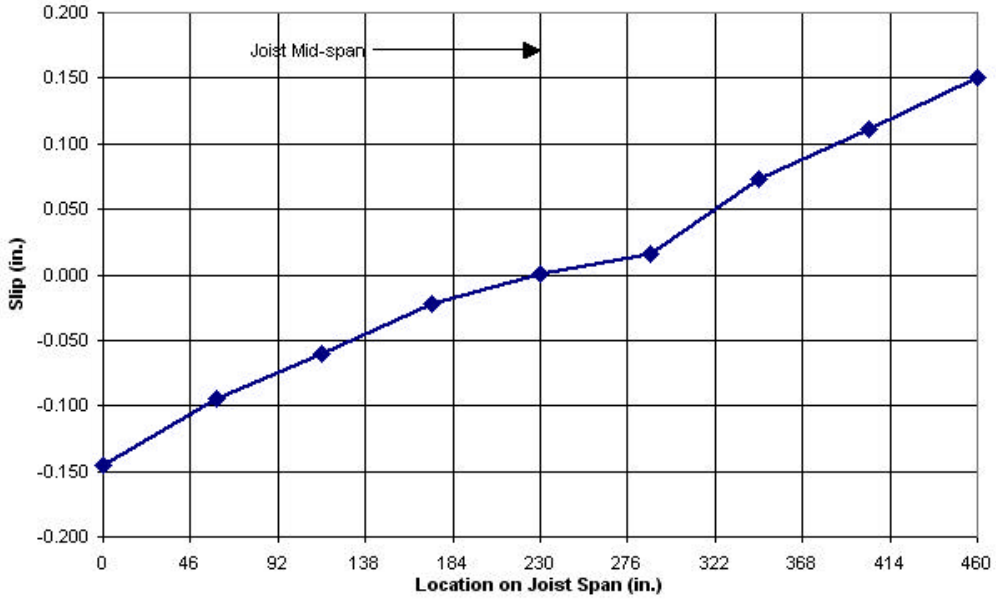

Fig. H.24 Test CSJ-13 Slip at Maximum Load

Intuitively, the problem could be bypassed by locating most connectors in regions with high shear, but this may be difficult and virtually impossible when high number of connectors is required. Therefore, it was necessary to develop design criteria that lead to a ductile shear connection.

A simple, but effective way to design a composite joist with a ductile shear connection is to insure in the course of the design procedure that the slip capacity of shear

connection, S_{max}, is not less than the required slip, S_u, of the composite joist being considered. One of the methods used to compute S_u was developed by Oehlers and Sved (1995). This method was developed for simply supported beams, and it hinges on recognition that steel and concrete components of a composite cross section are plastic in the central region of the beam, and elastic close to the support, and that just the opposite is true of shear connection. A rigorous derivation of the model for prediction of S_u is given by Oehlers and Sved (1995). The models developed by Oehlers and Sved were modified slightly in this study to make them applicable to composite joists, and are shown as Eqs. H.10 and H.11. The former applies to joists with distributed load, and the later is a general case that can be used for both concentrated forces and distributed load. The moment of inertia of joist can be calculated as given by Murray et al. (1997). That method is valid for $24 \geq L/d \geq 6$ if angle webs are used, or for $24 \geq L/d \geq 10$ if continuous round rod webs are used.

$$S_u = \frac{M_{max} L K_1}{3} - \frac{Q_M L K_2}{4} \qquad \text{(Eq. H.10)}$$

where:

M_{max} = maximum applied moment, Nmm

K_1 = $\dfrac{t_s + d_{jc} - a/2}{(EI)_{slab,eff.} + (EI)_{joist}}$, $(Nmm)^{-1}$

d_{jc} = distance between joist top and joist centroid, mm

a = depth of concrete stress block, mm

$I_{slab,eff}$ = moment of inertia corresponding to effective slab width and depth a, mm^4

I_{joist} = $C_r I_{chords}$

K_2 = $\dfrac{\left(t_s + d_{jc} - a/2\right)^2}{(EI)_{slab,eff} + (EI)_{joist}} + \dfrac{1}{(EA)_{joist}} + \dfrac{1}{(EA)_{slab,eff}}$

C_r = $0.90\left(1 - e^{-0.28(L/d)}\right)^{2.8}$ for joist with angle web members

= $0.721 + 0.00725(L/d)$ for joists with continuous rod web members

Q_M = force in shear connectors at M_{max}, N

$$S_u = A_m K_1 - A_{sh} K_2 \qquad \text{(Eq. H.11)}$$

where:

A_m = area under moment diagram between support and point of maximum moment, Nmm^2

A_{sh} = area under longitudinal shear force diagram between support and point of Maximum moment, Nmm

Slip data obtained from the tests was highly variable, and the effects of various parameters on slip were generally not clearly discernable from test data. The average measured slips for ribbed slabs were 16.7 mm for pullout failures, 15.4 mm for screw shear failures, and 7.9 mm for concrete rib failures. Values of C.O.V. associated with these slips were 16.6%, 39.8%, and 81.9%, respectively. Average measured slip for solid slab tests was 11.4 mm with C.O.V. of 38.2%. Clearly, the most ductile failures are associated with screw pullout failures, closely followed with screw shear, while the least ductility is associated with concrete rib failures. It can also be seen that the lower the slip, the higher the C.O.V., making the possible prediction thereof more difficult. While an accurate prediction of slip for various failures is difficult, approximate expressions were generated using numerical modeling. The power coefficients and constants in those expressions were than adjusted for the best fit with experimental data. Appropriately simplified equations for screw pullout, screw shear, and concrete rib failures in slabs with ribs perpendicular to the joist are given as Eqs. H.12, H.13, and H.14, respectively. Eq. H.15 can be used to calculate slips in solid slabs, and where ribs are parallel to the joist. The C.O.V values for these four equations are 15.5%, 34.7%, 48.5%, and 34.6%. Table H.5 shows the required and available slip computed for the full-scale test specimens. As can be seen, both CSJ-11 and CSJ-13 exhibited a lack of slip capacity. Both collapsed by premature failure of shear connection and therefore, their strengths are significantly over-predicted. The tests with sufficient slip capacities, CSJ-9, CSJ-10, and CSJ-12, are fairly accurately predicted. The test CSJ-8 failed by top chord buckling due to scarce spacing of screws, and its results should in this respect be disregarded.

Table H.5 Strength and Ductility Calculations in Full-Scale Tests

Test	M_{ta} (kN-m)	M_n (kN-m)	M_{ta}/M_n	S_u (mm)	S_{max} (mm)
CSJ-8	141.9	159.9	0.89	11	18
CSJ-9	185.6	187.6	0.99	7	17
CSJ-10	50.9	52.8	0.96	1	16
CSJ-11	520.3	559.3	0.93	14	11
CSJ-12	180.4	175.4	1.03	4	17
CSJ-13	860.8	1070.9	0.80	13	10

$$S_{max,\,sp} = \frac{1}{12}\sqrt{\frac{E_c}{f_c'}}D_e \qquad \text{(Eq. H.12)}$$

$$S_{max,\,ss} = 1.25\left(\frac{H_s}{t_{tc}}\right)^{0.8}\left(\frac{F_{ut,sc}}{E_s}\right)^{2/3}\frac{(w_{tc})^{1.2}}{(w_{r1})^{0.3}}(D_e)^{0.1} \qquad \text{(Eq. H.13)}$$

$$S_{max,\,crf} = 0.24\sqrt{\left(\frac{E_c}{f_c'}\right)\left(\frac{w_{r1}+w_{r2}}{2}\right)\left(\frac{H_s}{h_r}\right)}\left(\frac{Q_n}{s_{sc}^{3/4}F_{y,tc}}\right)^2\frac{1}{(w_{tc})(t_{tc})} \qquad \text{(Eq. H.14)}$$

where:

s_{sc} = minimum screw spacing, mm

= 16.5 mm for ELCO Grade 8 standoff screw

$$S_{max,\,solid} = \frac{1}{386}\left(\frac{E_c}{f_c'}\right)\left(\frac{w_{tc}}{t_{tc}}\right)^{0.5}\left(\frac{F_{ut,sc}}{E_s}\right)^{0.3}D_e \qquad \text{(Eq. H.15)}$$

H.6 RELIABILITY REQUIREMENTS

This part of the study consisted of determination of the strength reduction factor for joist flexural strength, ϕ_b, and slip capacity reduction factor, η_s.

The resistance factors were determined using the first-order, second-moment, probabilistic method. This simplified method uses two pieces of statistical information, means and coefficients of variation (C.O.V.). Reliability (ß) is the relationship between these two measures (Galambos and Ravindra 1973). This method was first developed by Cornell (1969) and Ravindra et al. (1969). The criteria used to calculate resistance factors for steel structures and composite beams was defined in a detail by Galambos and Ravindra (1973,

1976). The resistance factor was computed using Eq. H.16. Consistent with the previous work of Galambos and Ravindra (1973), the separation coefficient, a = 0.55, and reliability, ß = 3.0.

$$\phi_b = \frac{M_m}{M_n} e^{(-\alpha\beta V_R)} \qquad \text{(Eq. H.16)}$$

Statistical characteristics for concrete are given by Galambos and Ravindra (1976). In the absence of more specific data reflecting statistical characteristic of joist angle steel yield strength, the study employed average values of hot rolled beam web and flanges, as given by Galambos and Ravindra (1978a). Statistical information on the strength of high strength A490 bolts was taken from Galambos and Ravindra (1978b). Given a relatively small database of standoff screw tests, the characteristics of A490 bolts were used in the analysis. All the properties used are summarized as follows:

Joist Steel: $\left(F_y\right)_m = 1.08F_y,\ V_{F_y} = 0.11,\ \sigma_{F_y} = \left(F_y\right)_m V_{F_y} = 0.12F_y$

Concrete: $\left(f_c^{'}\right)_m = 1.17f_c^{'},\ V_{f_c^{'}} = 0.22,\ \sigma_{f_c^{'}} = 0.26f_c^{'}$

Standoff Screws: $\left(F_u\right)_m = 1.07F_u,\ V_{F_u} = 0.02,\ \sigma_{F_u} = 0.02F_u$

In the following analysis, the top and bottom chords are considered to be of the same strength, i.e. $F_{y,bc} = F_{y,tc} = F_y$. This assumption should be of no consequence for the reliability analysis, as statistical properties of the steel for both members are the same. The flexural strength of a fully composite joist is given by Eq. H.17.

$$M_n = A_{joist}F_y\left(t_s + d - \frac{A_{joist}F_y}{1.7f_c^{'}b_{eff}}\right) \qquad \text{(Eq. H.17)}$$

Having introduced $\xi_1 = \frac{A_{joist}F_y}{0.85b_{eff}t_sf_c^{'}}$, and $\xi_2 = \frac{d}{t_s}$, we can write:

$$\frac{M_m}{M_n} = \left[\frac{M_{ta}}{M_n}\right]_m \left\{ \frac{\frac{(F_y)_m}{(F_y)_n}\left[1 + \frac{\xi_2}{2} - \frac{(F_y)_m (f_c')_n}{(F_y)_n (f_c')_m}\frac{\xi_1}{2}\right]}{1 + \frac{\xi_2 - \xi_1}{2}} \right\} \qquad \text{(Eq. H.18)}$$

The parameter ξ_1 was investigated in its theoretical range from zero to one. The value of ξ_2 is not theoretically constrained, however, in this study it was investigated in the range of values from one to eight, as those two values were determined to be the limits of practical applications. The parameter $[M_{ta}/M_n]_m$ equals 0.99, and was calculated based on three full scale tests. The remaining three tests were excluded, as CSJ-8 failed due to top chord buckling, while CSJ-11 and CSJ-13 failed due to insufficient slip capacity of their shear connection. The standard deviation associated with materials was determined as shown by Eq. H.19. In determination of required statistical parameters, all variables involved in determining the strength of a composite joist were considered independent. Further, all geometric parameters of the joist and slab (i.e., slab thickness, effective slab width, top and bottom angle cross-sectional areas, joist depth, etc.) are assumed to be deterministic. Any variability in these parameters was considered covered within V_F.

$$\sigma_M = \sqrt{\left(\frac{\partial M_n}{\partial F_y}\right)_m^2 \sigma_{F_y}^2 + \left(\frac{\partial M_n}{\partial f_c'}\right)_m^2 \sigma_{f_c'}^2} \qquad \text{(Eq. H.19)}$$

V_M represents the C.O.V. for material properties and was calculated using Eq. H.20. Consistent with earlier recommendations by Galambos and Ravindra (1973), the C.O.V. due to fabrication imperfections, V_F, was assumed as 0.05. The professional C.O.V., V_P, represents variation in design theory, and is derived directly from comparison of theoretical calculations and tested data. In this case, $V_P = 0.04$. The overall C.O.V. for resistance, V_R, was determined with Eq. H.21.

$$V_M = \frac{\sqrt{\left[1+\frac{\xi_2}{2}-\frac{(F_y)_m (f_c')_n}{(F_y)_n (f_c')_m}\frac{\xi_1}{2}\right]^2 \sigma_{F_y}^2 + \left[\frac{\xi_1}{2}\frac{(F_y)_m^2 (f_c')_n^2}{(F_y)_n^2 (f_c')_m^2}\right]^2 \sigma_{f_c'}^2}}{\frac{(F_y)_m}{(F_y)_n}\left[1+\xi_2-\frac{(F_y)_m (f_c')_n}{(F_y)_n (f_c')_m}\frac{\xi_1}{2}\right]} \qquad \text{(Eq. H. 20)}$$

$$V_R = \sqrt{V_M^2 + V_F^2 + V_P^2 + V_M^2 V_F^2 + V_M^2 V_P^2 + V_F^2 V_P^2 + V_M^2 V_F^2 V_P^2} \qquad \text{(Eq. H.21)}$$

To determine the effect of shear connection on the resistance factor, it was first necessary to define the required statistical parameters pertaining to its strength. The effects of shear connection were considered for all three types of failure, and an average value of ϕ_b was computed. Eqs. H.22 through H.28 show how the values of $(Q_n)_m/(Q_n)_n$ and V_{Q_n} were calculated for concrete rib failure, and what the required adjustments are for Eqs. H.18 and H.20 to include the effect of shear connection.

$$(Q_n)_m = \left(\frac{Q_e}{Q_n}\right)_m \left[\frac{8.75\left(0.75\sqrt{1.17 f_c'}\right) D_e L_{fp}}{N^{2/3}}\right] \qquad \text{(Eq. H.22)}$$

and by combining the Eqs. H.7 and H.22, it can be written:

$$\frac{(Q_n)_m}{(Q_n)_n} = 1.11 \qquad \text{(Eq. H.23)}$$

Finally, the value of V_{Q_n} is computed as follows:

$$V_{Q_n} = \sqrt{V_P^2 + V_{(f_c')^{0.50}}^2} \qquad \text{(Eq. H.24)}$$

where:

$$V^2_{(f'_c)^{0.50}} = \frac{\left(\frac{\partial Q_n}{\partial f'_c}\right)^2 \sigma^2_{f'_c}}{(Q_n)^2_m} \qquad \text{(Eq. H.25)}$$

The expression for the nominal strength in terms of shear connection strength is then rewritten to result in Eq. H.26. Following a similar analysis as given above, the expressions for $(M)_m/(M)_n$ and V_M are given as Eq. H.27 and H.28, respectively.

$$(M_n)_n = A_{joist} F_y \left[t_s + \frac{d}{2} - \frac{\Sigma Q_n}{1.7 f'_c b_{eff}} \right] \qquad \text{(Eq. H.26)}$$

$$\frac{(M_n)_m}{(M_n)_n} = \left[\frac{M_{ta}}{M_n}\right]_m \left\{ \frac{\frac{(F_y)_m}{(F_y)_n}\left[1 + \frac{\xi_2}{2} - \frac{(Q_u)_m (f'_c)_n}{(Q_u)_n (f'_c)_m}\frac{\xi_1}{2}\right]}{1 + \frac{\xi_2 - \xi_1}{2}} \right\} \qquad \text{(Eq. H.27)}$$

$$V_M = \frac{\sqrt{\left[\frac{(F_y)_m (f'_c)_n}{2(F_y)_n (f'_c)_m}\xi_1\right]^2 \sigma^2_{Q_u} + \left[1 + \frac{\xi_2}{2} - \frac{(Q_u)_m (f'_c)_n}{(Q_u)_n (f'_c)_m}\frac{\xi_1}{2}\right]^2 \sigma^2_{F_y} + \left[\frac{\xi_1}{2}\frac{(F_y)_m (f'_c)_n (Q_u)_m}{(F_y)_n (f'_c)_m (Q_u)_n}\right]^2 \sigma^2_{f'_c}}}{\frac{(F_y)_m}{(F_y)_n}\left[1 + \xi_2 - \frac{(Q_u)_m (f'_c)_n}{(Q_u)_n (f'_c)_m}\frac{\xi_1}{2}\right]} \qquad \text{(Eq. H.28)}$$

When the effect of shear connection is not considered, the average computed value of ϕ_b equals 0.89, based on 143 considered cases. The general trend observed was that the value of ϕ_b decreases with a decreasing t_s/d ratio, and it increases with an increasing value of ξ_1. With respect to the effect of shear connection, with the same number of cases considered, it was found that computed values of ϕ_b vary by no more than 0.5% among the three modes of failure modes of failure, with an average of 0.87. If the two analysis (i.e. with and without the effect of shear connection) are combined, and if the value of ϕ_b is rounded off to the nearest 0.05 increment, the value of 0.90 is obtained. It is likely that the strength reduction factor would be somewhat higher had more full-scale test results been available. Further, the

recent reliability study for composite beams (Mujagic and Easterling 2004) shows that full-scale composite beams result in significantly higher strength reduction factors then those with a lesser degree of composite action, and it is a common practice to design composite joists as fully composite. Therefore, it is believed that $\phi_b = 0.90$ can be used safely.

Due to significant scatter in slip data, it was necessary to develop a slip reduction factor. Its role is to compensate for variation in slip data and ensure an adequate reliability of predicted ductility. The determination of η_s was performed with the process and reliability theory identical to that used to determine ϕ_b. Calculated values of η_s are summarized in Table H.6. As can be seen, most values of η_s are relatively low. Aside from previously discussed statistical scatter, nominal average over-strengths in steel and concrete were shown to be a major additional cause for lower values of η_s. For instance, while average over-strengths of 17% associated with concrete compressive strength has a favorable impact on strength and ϕ_b, but it has an unfavorable effect on slip and η_s.

Table H.6 Slip Capacity Reduction Factors

TYPE OF FAILURE	η_s
Screw Pullout	0.75
Screw Shear (ribbed slab)	0.60
Concrete Rib Failure	0.25
Screw Shear (solid slab)	0.55

While both S_u and S_{max} depend on a number of design parameters, making it possible to design a relatively long joist with a relatively small slip capacity demand, it is clear that concrete rib failures will by enlarge be limited to shorter members. This is due to both, smaller slip capacity and associated statistical scatter.

H.7 NUMERICAL EXAMPLE

The following example illustrates the procedure used to calculate flexural strength of a composite joists featuring standoff screws as shear connection. The joist is an interior member of a floor system with typical joist spacing, S_b, of 1.3 m. Various geometric properties not previously defined are shown in Fig. H.25.

STANDOFF SCREWS

H_s = 51 mm
D = 7.9 mm
$F_{ut,sc}$ = 1034 MPa

SLAB

t_s = 76 mm, h_r = 25 mm,
w_{r1} = 23 mm, w_{r2} = 70 mm
w_c = 2400 kg/m^3
f'_c = 25 MPa
w_{deck} = 50 Pa

JOIST

d = 500 mm, L = 9.0 m
Top chord: 2L-51x51x3.2
Bottom chord: 2L-64x64x6.4
$\bar{y}_t = 3.10$ mm , $\bar{y}_b = 6.08$ mm
$F_y = F_{y,bc} = F_{y,tc}$ = 248 MPa

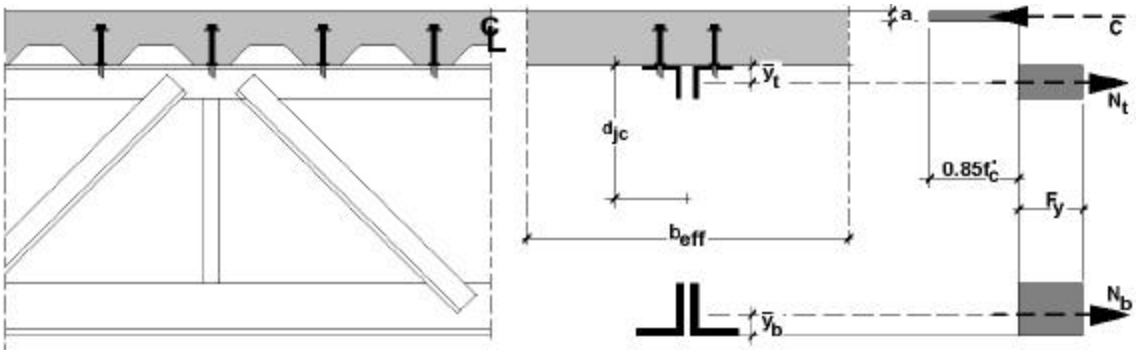

Fig. H.25 Configuration of the Example Composite Joist

First, the effective slab width is determined. It is the minimum of joist spacing and one quarter of joist span:

$$b_{eff} = \min\left\{\begin{matrix} S_b = 1300\,\text{mm} \\ L/4 = 9000/4 = 2250\,\text{mm} \end{matrix}\right\} = 1300\,\text{mm}$$

Next, forces in top and bottom chord due to dead weight of non-composite system, N_{tD} and N_{bD}, are determined:

$$w_D = w_{joist} + w_{deck} + w_{slab} = 0.25 + \left(\frac{50}{1000}\right)\left(\frac{1300}{1000}\right) + \left(\frac{2400(9.81)}{1000}\right)\left(\frac{51+25/2}{1000}\right)\left(\frac{1300}{1000}\right)$$

$$w_D = 2.26\,\text{kN/m} \rightarrow M_D = w_D L^2/8 = (2.26)(9)^2/8 = 22.87\,\text{kNm}$$

$$N_{tD} = N_{bD} = \frac{M_D}{d - \bar{y}_b - \bar{y}_t} = \frac{22.87(1000)}{500 - 3.10 - 6.08} = 46.60\,\text{kN}$$

Corresponding stresses in top and bottom chord, f_{tD} and f_{bD}, respectively, are:

$f_{tD} = 46.60(1000)/632 = 73.73\,\text{MPa}\,(\text{C})$, and $f_{bD} = 46.60(1000)/1560 = 29.87\,\text{MPa}\,(\text{T})$

Strength of shear connection in a half-span is computed next using Eq. H.9:

$$A_e = (\pi/4)(D - 24.75/n)^2 = (\pi/4)(7.9 - 24.75/24)^2 = 37.05\,\text{mm}^2$$

$$C_{tc} = \frac{1}{4}\sqrt{\frac{w_{tc}}{t_{tc}}} = \frac{1}{4}\sqrt{\frac{51}{3.2}} \approx 1.0$$

$$f_{ce} = 0.75\sqrt{f_c'} = 0.75\sqrt{30} = 4.11\text{MPa}$$

$$L_{fp} = L_s + 2\sqrt{\left(\frac{w_{r2} - L_s}{2}\right)^2 + \left(H_s - h_r\right)^2} = 2\sqrt{\left(\frac{70}{2}\right)^2 + \left(51 - 25\right)^2} = 87.2\text{mm}$$

$$Q_n = \min\left\{\begin{array}{c} 0.6C_{tc}A_eF_{ut,sc} = 0.6(1.0)(37.05)(1034)/1000 = 22.99\text{kN} \\ \dfrac{(D_e)^{1.6}(t_{tc})^{0.4}\sqrt{E_sF_{y,tc}}}{17.2} = \dfrac{(6.9)^{1.6}(3.2)^{0.4}\sqrt{200000(248)}}{17.2(1000)} = 14.34\text{kN} \\ \dfrac{8.75f_{ce}D_eL_{fp}}{N^{2/3}} = \dfrac{8.75(4.11)(6.9)(87.2)}{2^{2/3}} = 13.63\text{kN} \end{array}\right\} = 13.63\text{kN}$$

$$\Sigma Q_n = 38(13.63) = 517.94\text{kN}$$

Initially assuming that the joist is fully composite, i.e. $\Sigma Q_n \geq N_t + N_b$, the forces in the top and bottom chords, N_t and N_b, respectively, are computed. After the initial assumption is checked, the composite moment, M_c is computed by summing section forces around an arbitrary point. The section stress blocks are illustrated in Fig. H.25. A_{tc} and A_{bc} are respective cross-sectional areas of top and bottom chords.

$$N_t = A_{tc}F_y = 632(248)/1000 = 156.74\text{kN}$$

$$N_b = A_{bc}\left(F_y - f_{bD}\right) = 1560(248 - 29.87)/1000 = 340.28\text{kN}$$

$156.74 + 340.28 = 497.02\text{kN} < 517.94\text{kN}$, thus the joist is fully composite.

$$M_c = N_b\left(d + t_s - \bar{y}_b - \frac{a}{2}\right) + N_t\left(t_s + \bar{y}_t - \frac{a}{2}\right)$$

$$a = \frac{N_t + N_b}{0.85f_c'b_{eff}} = \frac{(156.74 + 340.28)1000}{0.85(30)(1300)} = 12.0\text{mm}$$

$$M_c = \frac{340.28}{1000}\left(500 + 76 - 6.08 - \frac{12}{2}\right) + \frac{156.74}{1000}\left(76 + 3.10 - \frac{12}{2}\right) = 201.24\text{kNm}$$

The design strength of the joist is computed as follows:

$$M_n = M_D + M_c$$

$$\phi M_n = 0.90(22.87 + 201.24) = 201.70\text{kNm}$$

Finally, the member ductility is checked. The design slip capacity is found with Eq. H.14:

$$\eta_s S_{max,\,crf} = 0.25(0.24)\sqrt{\left(\frac{E_c}{f_c'}\right)\left(\frac{w_{r1}+w_{r2}}{2}\right)\left(\frac{H_s}{h_r}\right)\left(\frac{Q_n}{s_{sc}^{3/4}F_{y,tc}}\right)^2\frac{1}{(w_{tc})(t_{tc})}}$$

$$E_c = 0.043 w_c^{1.5}\sqrt{f_c'} = 0.043(2400)^{1.5}\sqrt{30} = 27691\text{MPa}$$

$$\eta_s S_{max,\,crf} = 0.25(0.24)\sqrt{\left(\frac{27691}{30}\right)\left(\frac{23+70}{2}\right)\left(\frac{51}{25}\right)\left(\frac{13.63(1000)}{16.5^{0.75}248}\right)^2\frac{1}{(51)(3.2)}} = 4.9\text{mm}$$

The required slip is found next using Eq. H.10:

$$S_u = \frac{M_{max}LK_1}{3} - \frac{Q_M LK_2}{4}$$

Because the exact loading is not stipulated in this example, the assumption will be made that $M_{max} = M_u = \phi M_n = 201.70\text{kNm}$. Consequently, $Q_M = N_t + N_b = 497.02\text{kN}$.

$$K_1 = \frac{t_s + d_{jc} - a/2}{(EI)_{slab,eff.} + (EI)_{joist}}$$

$$I_{slab,eff} = (1/12)(b_{eff})(t_s - h_r)^3 = (1/12)(1300)(76-25)^3 = 14.4\cdot 10^6\,\text{mm}^4$$

$$K_1 = \frac{76 + 352.4 - 12.0/2}{(27691\cdot 14.4\cdot 10^6) + (200000\cdot 108.35\cdot 10^6)} = 1.91\cdot 10^{-11}(\text{Nmm})^{-1}$$

$$K_2 = \frac{(t_s + d_{jc} - a/2)^2}{(EI)_{slab,eff} + (EI)_{joist}} + \frac{1}{(EA)_{joist}} + \frac{1}{(EA)_{slab,eff}}$$

$$I_{joist} = C_r I_{chords}$$

$$C_r = 0.90\left(1 - e^{-0.28(L/d)}\right)^{2.8} = 0.90\left(1 - e^{-0.28(9000/500)}\right)^{2.8} = 0.884$$

$$I_{joist} = 0.884(108.35\cdot 10^6) = 95.76\cdot 10^6\,\text{mm}^4$$

$$K_2 = 8.09\cdot 10^{-9} + \frac{1}{(200000\cdot 95.76\cdot 10^6)} + \frac{1}{[27691(1300\cdot 51)]} = 8.63\cdot 10^{-9}(\text{Nmm})^{-1}$$

$$S_u = \frac{(201.7\cdot 10^6)(9\cdot 1000)(1.91\cdot 10^{-11})}{3} - \frac{(497.02\cdot 1000)(9\cdot 1000)(8.63\cdot 10^{-9})}{4} = 1.9\text{mm}$$

Thus, since $\eta_s S_{max} \geq S_u$, the ductility requirements are satisfied.

H.8 SUMMARY AND CONCLUSIONS

Standoff screws represent an innovative and effective mean of shear connection. With their application, the need for bulky welding equipment at the job site and unnecessarily thick top chords can be minimized. The strength computation model derived in this study by means of experimental data and FEA predict the screw connection strength from three types of failure: screw shear, screw pullout, and concrete rib failure. In a particular design situation, computations for each mode of failure are performed, and the minimum governing strength represents the capacity of the connection and the nominal mode of failure.

A very important aspect of composite joists featuring standoff screws as shear connectors, and composite flexural members in general, is ductility of shear connection. It allows for redistribution of horizontal shear among the connectors through inelastic deformations of shear connectors along the span of the joist. The lack of ability of shear connection to sustain slip can result in premature failure as a result of the inability of bad to progressively transfer to subsequent connectors towards the middle of the span. A procedure was developed to predict the required and available slip of a particular joist member. Generally, brittle connections embodied in concrete rib failure have less slip capacity, and are more appropriate for shorter members.

Finally, a reliability study was performed for both, the strength prediction model and slip prediction equations to insure that proper safety performance of the procedure, and that it can be easily adopted into design codes.

H.9 REFERENCES

ACI. (2002). *Building Code Requirements for Structural Concrete (ACI 318-02) and Commentary (ACI 318R-02)*. American Concrete Institute, Farmington Hills, Michigan.

Alander, C.C., Easterling, W.S., and Murray, T.M. (1998). "Standoff Screws Used in Composite Joists." Report No. CE/VPI - ST 98/02, Virginia Polytechnic Institute and State University, Blacksburg, VA.

Carreira, D.J. and Chu, K.H. (1986). "Stress-Strain Relationship for Plain Concrete in Tension." *Journal of the American Concrete Institute*, ACI, 83(3), 21-28.

Cornell, C.A. (1969). "A Probability-Based Structural Code." *Journal of the American Concrete Institute*, ACI, 66(12), 974-985.

El-Lobody, E. and Lam, D. (2002). "Modelling of headed stud in steel-precast composite beams." *Steel & Composite Structures: An International Journal*, Techno-Press, Vol. 2, No. 5, 355-378.

Galambos, T.V., and Ravindra, M.K. (1973). Tentative Load and Resistance Factor Design Criteria for Steel Buildings. Research Report No. 18, Washington University, St. Louis, MO.

Galambos, T.V. and Ravindra, M.K. (1976). Load and Resistance Factor Design Criteria for Composite Beams. Research Report No. 44, Washington University, St. Louis, MO.

Galambos, T.V. and Ravindra, M.K. (1978a). "Properties of Steel for Use in LRFD." *Journal of the Structural Division*, ASCE, 104(9), 1459-1468.

Galambos, T.V. and Ravindra, M.K. (1978b). "Load and Resistance Factor Design Criteria for Connectors." *Journal of the Structural Division*, ASCE, 104(9), 1427-1441.

Hankins, S.C., Gibbings, D.R., Easterling, W.S. and Murray, T.M. (1994). "Standoff Screws Functioning as Shear Connectors in Composite Joists." Report CE/VPI-ST 94/16, Virginia Polytechnic Institute and State University, Blacksburg, VA.

Hibbitt, Karlsson & Sorensen, Inc. (2001a). ABAQUS/Standard User's Manual, Vol. II. HKS, Pawtucket, RI.

Hibbitt, Karlsson & Sorensen, Inc. (2001b). Analysis of Concrete Structures with ABAQUS. HKS, Pawtucket, RI.

Hibbitt, Karlson & Sorenson, Inc. (2003). ABAQUS – Standard, v. 6.3, HKS, Pawtucket, RI.

Hilleborg, A., Modéer, M. and Petersson, P.E. (1976). "Analysis of Crack Formation and Crack Growth in Concrete by means of Fracture Mechanics and Finite Elements," Cement and Concrete Research, Vol. 6, 773-782.

Jayas, B.S., and Hosain, M.U. (1987). "Behaviour of Headed Studs in Composite Beams: Push-out Tests." *Canadian Journal of Civil Engineering*, 15, 240-253.

Lauer, D.F., Gibbings, D.R., Easterling, W.S. and Murray, T.M. (1996). "Evaluation of Composite Short-Span Joists." Report CE/VPI-ST 96/06, Virginia Polytechnic Institute and State University, Blacksburg, VA.

Lin, C., and Scordelis, A.C. (1975). "Nonlinear Analysis of RC Shells of General Form," ASCE Journal of the Structural Division, Vol. 101, ST3, 523-538.

Mason, B. S., Easterling, W.S. and Murray, T.M. (2002). "Standoff Screws as Shear Connectors in Composite Joist Design." Report No. CE/VPI - ST 02/03, Virginia Polytechnic Institute and State University, Blacksburg, VA.

Mujagic J.R.U., Easterling, W.S. and Murray, T.M. (2000). "Further Investigation of Short Span Composite Joists." Report No. CE/VPI - ST 00/20, Virginia Polytechnic Institute and State University, Blacksburg, VA.

Mujagic, J.R.U., Easterling, W.S. and Murray, T.M. (2001). "Strength Calculation Model for Standoff Screws in Composite Joists." Report No. CE/VPI - ST 00/19, Virginia Polytechnic Institute and State University, Blacksburg, VA.

Mujagic, J.R.U., and Easterling, W.S. (2003). "Standoff Screws as Shear Connectors in Composite Joists: Results of Finite Element Analysis." Report No. CE/VPI - ST 03/12, Virginia Polytechnic Institute and State University, Blacksburg, VA.

Mujagic, J.R.U. and Easterling, W.S. (2004). "Reliability Assessment of Composite Beams." Chapter I of dissertation.

Murray, T.M., Allen, D.E., Ungar, E.E. (1997). "Floor Vibrations Due to Human Activity." AISC Steel Design Guide Series, No. 11, AISC, Chicago, IL.

Oehlers, D.J. and Sved, G. (1995). "Composite Beams with Limited Slip-Capacity Shear Connectors." *Journal of the Structural Engineering*, ASCE, Vol. 121, No. 6, 932-938.

Ravindra, M.K., Heaney, A.C., and Lind, N.C. (1969). "Probabilistic Evaluation of Safety Factors," Symposium on Concepts of Safety of Structures and Methods of Design, IABSE, London, UK.

Salmon, C.G. and Johnson, J.E. (1996). *Steel Structures: Design and Behavior*, Fourth Edition, Harper Collins, New York, NY.

Webler, J.E., Easterling, W.S. and Murray, T.M. (2000). "Further Investigation of Standoff Screws Used in Composite Joists." Report No. CE/VPI - ST 00/18, Virginia Polytechnic Institute and State University, Blacksburg, VA.

H.10 APPENDIX I

Table AH.1 Summary of Push-out Test Parameters and Results

Test No.	Deck	w_{r1} (mm)	w_{r2} (mm)	h_r (mm)	H_s (mm)	N	w_{tc} (mm)	t_{tc} (mm)	t_s (mm)	F_{ytc} (MPa)	F_{utc} (MPa)	l_s (mm)	f'_c (MPa)	R_t (kN)	Failure[c]
P-3-1	1.0C	23	70	25	51	1	31.8	3.1	102	394	586	87	29.0	17.2	SP
P-3-2	1.0C	23	70	25	51	1	31.8	3.1	102	394	586	87	28.3	16.4	SP
P-3-3	1.0C	23	70	25	51	1	31.8	3.1	102	394	586	87	29.6	15.7	SP
1-1-1	none	n/a	n/a	n/a	51	n/a	31.8	2.8	102	371	558	n/a	26.2	23.2	SS
1-1-3	none	n/a	n/a	n/a	51	n/a	31.8	2.8	102	371	558	n/a	26.2	24.5	SS
1-2-1	none	n/a	n/a	n/a	51	n/a	38.1	3.1	102	401	603	n/a	26.9	28.9	SS/SP
1-2-3	none	n/a	n/a	n/a	51	n/a	38.1	3.1	102	401	603	n/a	25.5	24.3	SS
1-3-1	none	n/a	n/a	n/a	51	n/a	38.1	4.3	102	383	578	n/a	24.1	27.1	SS
1-3-2	none	n/a	n/a	n/a	51	n/a	38.1	4.3	102	383	578	n/a	26.2	31.4	SS
1-4-1	none	n/a	n/a	n/a	51	n/a	50.8	5.2	102	398	588	n/a	23.4	32.2	SS
1-4-2	none	n/a	n/a	n/a	51	n/a	50.8	5.2	102	398	588	n/a	26.2	32.7	SS
1-4-3	none	n/a	n/a	n/a	51	n/a	50.8	5.2	102	398	588	n/a	26.2	33.8	SS
1-5-1	none	n/a	n/a	n/a	51	n/a	50.8	6.0	102	398	576	n/a	25.5	25.5	SS
1-5-2	none	n/a	n/a	n/a	51	n/a	50.8	6.0	102	398	576	n/a	26.2	27.8	SS
1-5-3	none	n/a	n/a	n/a	51	n/a	50.8	6.0	102	398	576	n/a	26.2	26.2	SS
2-1-1	0.6C	19	44	14	38	1	31.8	2.8	51	395	567	65	48.3	16.2	CRF
2-1-2	0.6C	19	44	14	38	1	31.8	2.8	51	395	567	65	48.3	16.1	CRF
2-1-3	0.6C	19	44	14	38	1	31.8	2.8	51	395	567	65	48.3	15.8	CRF
2-2-1	0.6C	19	44	14	38	1	38.1	3.9	51	376	550	65	48.3	17.8	CRF
2-2-2	0.6C	19	44	14	38	1	38.1	3.9	51	376	550	65	48.3	18.5	CRF
2-2-3	0.6C	19	44	14	38	1	38.1	3.9	51	376	550	65	48.3	17.7	CRF
2-3-1	0.6C	19	44	14	38	1	50.8	5.2	51	376	552	65	48.3	19.4	CRF
2-3-2	0.6C	19	44	14	38	1	50.8	5.2	51	376	552	65	48.3	17.3	CRF
2-3-3	0.6C	19	44	14	38	1	50.8	5.2	51	376	552	65	48.3	17.9	CRF
2-4-1	0.6C	19	44	14	38	1	50.8	6.4	51	356	532	65	48.3	16.9	CRF
2-4-2	0.6C	19	44	14	38	1	50.8	6.4	51	356	532	65	48.3	18.3	CRF
2-4-3	0.6C	19	44	14	38	1	50.8	6.4	51	356	532	65	48.3	16.5	CRF
3-1-1	1.0C	23	70	25	51	1	31.8	2.8	64	371	539	87	33.8	16.2	SP
3-1-2	1.0C	23	70	25	51	1	31.8	2.8	64	371	539	87	33.8	14.8	SP
3-1-3	1.0C	23	70	25	51	1	31.8	2.8	64	371	539	87	33.8	15.3	SP
3-2-1	1.0C	23	70	25	51	1	38.1	3.9	64	363	533	87	33.8	19.6	CRF
3-2-2	1.0C	23	70	25	51	1	38.1	3.9	64	363	533	87	33.8	19.5	CRF
3-2-3	1.0C	23	70	25	51	1	38.1	3.9	64	363	533	87	33.1	18.5	SS/SP
3-3-1	1.0C	23	70	25	51	1	50.8	5.2	64	401	587	87	31.7	21.2	CRF/SP
3-3-2	1.0C	23	70	25	51	1	50.8	5.2	64	401	587	87	31.7	19.6	SS/CRF
3-3-3	1.0C	23	70	25	51	1	50.8	5.2	64	401	587	87	31.7	20.8	SS/CRF
3-4-1	1.0C	23	70	25	51	1	50.8	6.4	64	358	543	87	33.1	18.6	SS/CRF
3-4-2	1.0C	23	70	25	51	1	50.8	6.4	64	358	543	87	31.7	16.5	SS/CRF
3-4-3	1.0C	23	70	25	51	1	50.8	6.4	64	358	543	87	31.7	19.9	CRF
4-1-1	1.5VL	44	64	38	51	1	31.8	2.8	102	371	558	68	37.2	17.7	CRF
4-1-2	1.5VL	44	64	38	51	1	31.8	2.8	102	371	558	68	37.2	19.1	CRF
4-1-3	1.5VL	44	64	38	51	1	31.8	2.8	102	371	558	68	37.2	19.3	SP/CRF
4-2-1	1.5VL	44	64	38	51	1	38.1	4.3	102	383	578	68	35.2	21.3	CRF
4-2-2	1.5VL	44	64	38	51	1	38.1	4.3	102	383	578	68	36.5	21.7	CRF
4-2-3	1.5VL	44	64	38	51	1	38.1	4.3	102	383	578	68	36.5	22.8	CRF
4-3-1	1.5VL	44	64	38	51	1	50.8	6.2	102	398	576	68	36.5	20.4	CRF
4-3-2	1.5VL	44	64	38	51	1	50.8	6.2	102	398	576	68	36.5	21.1	CRF
4-3-3	1.5VL	44	64	38	51	1	50.8	6.1	102	398	576	68	36.5	21.7	CRF
4-4-1	1.5VL	44	64	38	51	1	50.8	6.4	89	366	552	68	33.1	21.9	CRF
4-4-2	1.5VL	44	64	38	51	1	50.8	6.4	89	366	552	68	33.1	18.9	SS
4-4-3	1.5VL	44	64	38	51	1	50.8	6.4	89	366	552	68	33.1	21.6	CRF
5-1-1	1.5VL	44	64	38	64	1	31.8	2.8	89	395	567	81	30.3	22.3	SP
5-1-2	1.5VL	44	64	38	64	1	31.8	2.8	89	395	567	81	30.3	21.7	SP
5-1-3	1.5VL	44	64	38	64	1	31.8	2.8	89	395	567	81	30.3	22.3	SP
5-2-1	1.5VL	44	64	38	64	1	38.1	3.9	89	376	550	81	30.3	24.3	CRF
5-2-2	1.5VL	44	64	38	64	1	38.1	3.9	89	376	550	81	30.3	24.5	CRF
5-2-3	1.5VL	44	64	38	64	1	38.1	3.9	89	376	550	81	30.3	24.7	CRF
5-3-1	1.5VL	44	64	38	64	1	50.8	5.2	89	376	552	81	30.3	22.7	CRF/SS
5-3-2	1.5VL	44	64	38	64	1	50.8	5.2	89	376	552	81	30.3	24.3	SS
5-3-3	1.5VL	44	64	38	64	1	50.8	5.2	89	376	552	81	30.3	23.2	CRF

Table AH.1(cont'd) Summary of Push-out Test Parameters and Results

Test No.	Deck	w_{r1} (mm)	w_{r2} (mm)	h_r (mm)	H_s (mm)	N	w_{tc} (mm)	t_{tc} (mm)	t_s (mm)	F_{ytc} (MPa)	F_{utc} (MPa)	l_s (mm)	f'_C (MPa)	R_t (kN)	Failure[c]
P3-1	1.0C	23	70	25	76	2	50.8	4.7	83	401	576	124	28.3	20.9	SS
P3-2	1.0C	23	70	25	76	2	50.8	4.7	83	401	576	124	28.3	19.0	SS
P3-3	1.0C	23	70	25	76	2	50.8	4.7	83	401	576	124	28.3	19.0	SS
P4-1	1.0C	23	70	25	76	2	50.8	4.7	83	401	576	124	31.7	21.7	SS
P4-2	1.0C	23	70	25	76	2	50.8	4.7	83	401	576	124	31.7	18.5	SS
P4-3	1.0C	23	70	25	76	2	50.8	4.7	83	401	576	124	31.7	18.5	SS
P5-1	1.0C	23	70	25	76	1	50.8	4.7	83	401	576	124	36.5	22.9	SS
P5-2	1.0C	23	70	25	76	1	50.8	4.7	83	401	576	124	36.5	22.6	SS
P6-1	1.0C	23	70	25	76	1	50.8	4.7	83	401	576	124	36.5	23.0	SS
P6-2	1.0C	23	70	25	76	1	50.8	4.7	83	401	576	124	36.5	23.2	SS
P9-2	none	n/a	n/a	n/a	64	n/a	50.8	4.7	76	401	576	n/a	37.2	28.5	SS
P9-3	none	n/a	n/a	n/a	64	n/a	50.8	4.7	76	401	576	n/a	37.2	28.5	SS
P10-1	none	n/a	n/a	n/a	64	n/a	50.8	4.7	76	401	576	n/a	22.1	32.2	SS
P10-2	none	n/a	n/a	n/a	64	n/a	50.8	4.7	76	401	576	n/a	22.1	32.4	SS
~~P11-1~~	~~1.0C~~	~~23~~	~~70~~	~~25~~	~~76~~	~~2~~	~~50.8~~	~~4.7~~	~~83~~	~~401~~	~~576~~	~~124~~	~~22.1~~	~~14.9~~	~~SS~~
~~P11-2~~	~~1.0C~~	~~23~~	~~70~~	~~25~~	~~76~~	~~2~~	~~50.8~~	~~4.7~~	~~83~~	~~401~~	~~576~~	~~124~~	~~22.1~~	~~15.0~~	~~SS~~
A1-1	0.6C	19	44	14	51	1	31.8	2.8	57	410	543	85	33.1	19.7	SP
A1-2	0.6C	19	44	14	51	1	31.8	2.8	57	410	543	85	33.1	16.8	SP
A1-3	0.6C	19	44	14	51	1	31.8	2.8	57	410	543	85	37.9	20.8	SP
A2-1	0.6C	19	44	14	51	1	50.8	4.7	57	419	585	85	33.1	24.6	SS
A2-2	0.6C	19	44	14	51	1	50.8	4.7	57	419	585	85	33.1	23.7	SS
A5-1	0.6C	19	44	14	64	1	50.8	6.4	70	382	535	108	37.9	20.2	SS
A5-2	0.6C	19	44	14	64	1	50.8	6.4	70	382	535	108	37.9	18.3	SS
A6-1	0.6C	19	44	14	51	1	31.8	2.8	57	410	543	85	35.2	18.3	SP
A6-2	0.6C	19	44	14	51	1	31.8	2.8	57	410	543	85	35.2	18.3	SP
A7-1	0.6C	19	44	14	51	1	50.8	4.7	57	419	585	85	35.2	23.0	SS
A7-2	0.6C	19	44	14	51	1	50.8	4.7	57	419	585	85	35.2	24.1	SS
A8-1	0.6C	19	44	14	51	1	50.8	6.4	57	382	535	85	35.2	22.5	SS
A8-2	0.6C	19	44	14	51	1	50.8	6.4	57	382	535	85	35.2	23.2	SS
B1-1	1.0C	23	70	25	51	1	31.8	2.8	57	409	543	87	29.6	14.4	SP
B1-2	1.0C	23	70	25	51	1	31.8	2.8	57	409	543	87	29.6	13.7	SP
B2-1	1.0C	23	70	25	51	1	50.8	4.7	57	419	585	87	29.6	15.6	SS
B2-2	1.0C	23	70	25	51	1	50.8	4.7	57	419	585	87	29.6	16.3	SS
B3-1	1.0C	23	70	25	51	1	50.8	6.4	57	382	535	87	29.6	15.1	SS
B3-2	1.0C	23	70	25	51	1	50.8	6.4	57	382	535	87	29.6	14.3	SS
B4-1	1.0C	23	70	25	64	1	31.8	2.8	70	410	543	104	26.2	16.1	SP
B4-2	1.0C	23	70	25	64	1	31.8	2.8	70	410	543	104	26.2	17.4	SP
B5-1	1.0C	23	70	25	64	1	50.8	4.7	70	419	585	104	26.2	20.5	SS
B5-2	1.0C	23	70	25	64	1	50.8	4.7	70	419	585	104	26.2	20.4	SS
B6-1	1.0C	23	70	25	64	1	50.8	6.4	70	382	535	104	26.2	17.8	SS
B6-2	1.0C	23	70	25	64	1	50.8	6.4	70	382	535	104	26.2	17.5	SS
B7-1	1.0C	23	70	25	76	1	31.8	2.8	83	410	543	124	26.2	16.8	SP
B7-2	1.0C	23	70	25	76	1	31.8	2.8	83	410	543	124	26.2	16.2	SP
B8-1	1.0C	23	70	25	76	1	50.8	4.7	83	419	585	124	26.2	21.5	SS
B8-2	1.0C	23	70	25	76	1	50.8	4.7	83	419	585	124	26.2	21.5	SS
B9-1	1.0C	23	70	25	76	1	50.8	6.4	83	382	535	124	32.4	19.5	SS
B9-2	1.0C	23	70	25	76	1	50.8	6.4	83	382	535	124	32.4	19.5	SS
~~B10-1~~	~~1.0C~~	~~23~~	~~70~~	~~25~~	~~76~~	~~2~~	~~50.8~~	~~4.1~~	~~83~~	~~410~~	~~570~~	~~124~~	~~32.4~~	~~15.6~~	~~SS~~
B11-1	1.0C	23	70	25	76	2	76.2	8.0	83	399	569	124	33.1	13.3	SS
B11-2	1.0C	23	70	25	76	2	76.2	8.0	83	399	569	124	33.1	14.2	SS
B12-1	1.0C	23	70	25	64	1	31.8	2.8	70	383	530	104	45.5	15.9	CRF/SP
B12-2	1.0C	23	70	25	64	1	31.8	2.8	70	383	530	104	45.5	18.2	CRF/SP
B13-1	1.0C	23	70	25	64	1	50.8	4.7	70	427	590	104	48.3	24.6	CRF/SS
B13-2	1.0C	23	70	25	64	1	50.8	4.7	70	427	590	104	48.3	21.7	CRF/SS
B14-1	1.0C	23	70	25	64	2	31.8	2.8	70	383	530	104	44.8	16.2	CRF/SP
B14-2	1.0C	23	70	25	64	2	31.8	2.8	70	383	530	104	44.8	16.5	CRF/SP
B14R-1	1.0C	23	70	25	64	2	31.8	2.8	70	383	530	104	40.7	16.7	CRF/SP
B14R-2	1.0C	23	70	25	64	2	31.8	2.8	70	383	530	104	40.7	16.5	CRF/SP
B14RR-1	1.0C	23	70	25	64	2	31.8	2.8	76	383	530	104	35.2	16.3	SP
B14RR-2	1.0C	23	70	25	64	2	31.8	2.8	76	383	530	104	35.2	17.0	SP
B15-1	1.0C	23	70	25	64	2	50.8	4.7	70	427	590	104	46.2	21.1	CRF/SS
B15-2	1.0C	23	70	25	64	2	50.8	4.7	70	427	590	104	46.2	22.3	CRF/SS
B15R-1	1.0C	23	70	25	64	2	50.8	4.7	76	427	590	104	37.9	23.0	CRF/SS
B15R-2	1.0C	23	70	25	64	2	50.8	4.7	76	427	590	104	37.9	22.7	CRF/SS
B15RR-1	1.0C	23	70	25	64	2	50.8	4.7	76	427	590	104	35.2	19.8	SS
B15RR-2	1.0C	23	70	25	64	2	50.8	4.7	76	427	590	104	35.2	20.5	SS

Table AH.1(cont'd) Summary of Push-out Test Parameters and Results

Test No.	Deck	w_{r1} (mm)	w_{r2} (mm)	h_r (mm)	H_s (mm)	N	w_{tc} (mm)	t_{tc} (mm)	t_s (mm)	F_{ytc} (MPa)	F_{utc} (MPa)	l_s (mm)	f'c (MPa)	R_t (kN)	Failure[c]
B16-1	1.0C	23	70	25	64	2	50.8	6.4	70	389	531	104	50.3	14.7	CRF/SS
B16-2	1.0C	23	70	25	64	2	50.8	6.4	70	389	531	104	50.3	15.3	CRF/SS
B16R-1	1.0C	23	70	25	64	2	50.8	6.4	76	389	531	104	37.9	14.8	CRF/SS
B16R-2	1.0C	23	70	25	64	2	50.8	6.4	76	389	531	104	37.9	13.6	CRF/SS
B16R-3	1.0C	23	70	25	64	2	50.8	6.4	76	389	531	104	37.9	13.0	CRF/SS
B16RR-1	1.0C	23	70	25	64	2	50.8	6.4	76	389	531	104	34.5	16.0	SS
B16RR-2	1.0C	23	70	25	64	2	50.8	6.4	76	389	531	104	34.5	15.8	SS
B17-1	1.0C	23	70	25	64	1	31.8	2.8	76	396	538	104	31.7	20.4	SP
B17-2	1.0C	23	70	25	64	1	31.8	2.8	76	396	538	104	31.7	19.0	SP
B18-1	1.0C	23	70	25	64	1	38.1	3.5	76	412	550	104	19.3	18.0	SS/SP
B18-2	1.0C	23	70	25	64	1	38.1	3.5	76	412	550	104	19.3	18.0	SS/SP
B19-1	1.0C	23	70	25	64	1	38.1	3.9	76	402	536	104	19.3	18.7	SS
B19-2	1.0C	23	70	25	64	1	38.1	3.9	76	402	536	104	19.3	19.6	SS
B20-1	1.0C	23	70	25	64	1	38.1	4.3	76	420	574	104	24.8	21.6	CRF
B20-2	1.0C	23	70	25	64	1	38.1	4.3	76	420	574	104	24.8	20.9	SS
B21-1	1.0C	23	70	25	64	1	50.8	4.7	76	386	516	104	33.1	23.4	SS
B21-2	1.0C	23	70	25	64	1	50.8	4.7	76	386	516	104	33.1	25.5	SS
B22-1	1.0C	23	70	25	64	1	50.8	6.4	76	420	590	104	19.3	16.9	SS
B22-2	1.0C	23	70	25	64	1	50.8	6.4	76	420	590	104	19.3	15.6	SS
C1-1	1.5C	89	108	38	76	1	31.8	2.8	83	410	543	132	40.0	18.0	SS
C1-2	1.5C	89	108	38	76	1	31.8	2.8	83	410	543	132	40.0	18.0	SS
C1R-1	1.5C	89	108	38	76	1	31.8	2.8	83	383	530	132	28.3	24.0	SS
C1R-2	1.5C	89	108	38	76	1	31.8	2.8	83	383	530	132	28.3	20.7	SS
C1R-3	1.5C	89	108	38	76	1	31.8	2.8	83	383	530	132	28.3	22.5	SS
C2-1	1.5C	89	108	38	76	1	50.8	4.7	83	419	585	132	40.0	23.0	SS
C2-2	1.5C	89	108	38	76	1	50.8	4.7	83	419	585	132	40.0	23.8	SS
C2R-1	1.5C	89	108	38	76	1	50.8	4.7	83	427	590	132	28.3	26.1	SS
C2R-2	1.5C	89	108	38	76	1	50.8	4.7	83	427	590	132	28.3	25.3	SS
C3-1	1.5C	89	108	38	76	1	50.8	6.4	83	382	536	132	29.6	20.9	SS
C3-2	1.5C	89	108	38	76	1	50.8	6.4	83	382	536	132	29.6	18.3	SS
C4-1	1.5C	89	108	38	76	2	31.8	2.8	83	410	543	132	29.6	18.9	SS/SP
C4-2	1.5C	89	108	38	76	2	31.8	2.8	83	410	543	132	29.6	20.3	SP
C5-1	1.5C	89	108	38	76	2	50.8	4.7	83	419	585	132	29.6	24.5	SS/CRF
C5-2	1.5C	89	108	38	76	2	50.8	4.7	83	419	585	132	29.6	25.2	SS/CRF
C6-1	1.5C	89	108	38	76	2	50.8	6.4	83	382	535	132	29.6	20.3	SS/CRF
C6-2	1.5C	89	108	38	76	2	50.8	6.4	83	382	535	132	29.6	18.3	SS
C7-1	1.5C	89	108	38	89	4	50.8	4.1	95	410	570	158	29.6	17.3	SS/CRF
C7-2	1.5C	89	108	38	89	4	50.8	4.1	95	410	570	158	29.6	21.1	SS
C8-1	1.5C	89	108	38	89	4	50.8	6.4	95	382	535	158	26.9	18.1	SS
C8-2	1.5C	89	108	38	89	4	50.8	6.4	95	382	535	158	26.9	16.1	SS
C9-1	1.5C	89	108	38	76	4	50.8	4.1	89	394	537	139	37.2	15.2	CRF
C9-2	1.5C	89	108	38	76	4	50.8	4.1	89	394	537	139	37.2	13.7	CRF
C9R-1	1.5C	89	108	38	76	4	50.8	4.1/6.4[a]	89	394	537	139	30.3	15.3	CRF
C9R-2	1.5C	89	108	38	76	4	50.8	4.1/6.4[a]	89	394	537	139	30.3	15.7	CRF
C10-1	1.5C	89	108	38	76	4	50.8	6.4	89	376	534	139	37.2	15.3	CRF
C10-2	1.5C	89	108	38	76	4	50.8	6.4	89	376	534	139	37.2	16.6	CRF
C10R-1	1.5C	89	108	38	76	4	50.8	6.4	89	376	534	139	29.0	17.6	CRF
C10R-2	1.5C	89	108	38	76	4	50.8	6.4	89	376	534	139	29.0	16.0	CRF
C10R-3	1.5C	89	108	38	76	4	50.8	6.4	89	376	534	139	29.0	16.5	CRF
C11-1	1.5C	89	108	38	76	1	50.8	6.4	89	447	598	132	24.8	22.0	SS
C11-2	1.5C	89	108	38	76	1	50.8	6.4	89	447	598	132	24.8	20.1	SS
D1-1	1.5VL	44	64	38	76	1	31.8	2.8	83	410	543	99	24.8	18.2	SP
D1-2	1.5VL	44	64	38	76	1	31.8	2.8	83	410	543	99	24.8	17.3	SP
D2-1	1.5VL	44	64	38	76	1	50.8	4.7	83	419	585	99	24.8	25.8	SS
D2-2	1.5VL	44	64	38	76	1	50.8	4.7	83	419	585	99	24.8	24.5	SS
D3-1	1.5VL	44	64	38	76	1	50.8	6.4	83	382	535	99	24.8	21.0	SS
D3-2	1.5VL	44	64	38	76	1	50.8	6.4	83	382	535	99	24.8	25.0	SS
D4-1	1.5VL	44	64	38	76	2	31.8	2.8	83	410	543	99	24.8	18.3	SP
D4-2	1.5VL	44	64	38	76	2	31.8	2.8	83	410	543	99	24.8	17.7	SP
D5-1	1.5VL	44	64	38	76	2	50.8	4.7	83	419	585	99	37.2	24.3	CRF
D5-2	1.5VL	44	64	38	76	2	50.8	4.7	83	419	585	99	37.2	19.2	CRF
D5R-1	1.5VL	44	64	38	76	2	50.8	4.7	89	427	590	99	22.1	18.7	CRF
D5R-2	1.5VL	44	64	38	76	2	50.8	4.7	89	427	590	99	22.1	18.5	CRF
D6-1	1.5VL	44	64	38	76	2	50.8	6.4	83	382	536	99	37.2	18.2	CRF
D6-2	1.5VL	44	64	38	76	2	50.8	6.4	83	382	536	99	37.2	18.2	CRF

Table AH.1(cont'd) Summary of Push-out Test Parameters and Results

Test No.	Deck	w_{r1} (mm)	w_{r2} (mm)	h_r (mm)	H_s (mm)	N	w_{tc} (mm)	t_{tc} (mm)	t_s (mm)	F_{ytc} (MPa)	F_{utc} (MPa)	l_s (mm)	f'_c (MPa)	R_f (kN)	Failure[c]
D6R-1	1.5VL	44	64	38	76	2	50.8	6.4	89	376	534	99	21.4	16.8	SS
D6R-2	1.5VL	44	64	38	76	2	50.8	6.4	89	376	534	99	21.4	18.5	SS
D7-1	1.5VL	44	64	38	76	4	50.8	4.1	95	415	550	105	37.2	10.5	CRF
D7-2	1.5VL	44	64	38	76	4	50.8	4.1	95	415	550	105	37.2	9.6	CRF
D7R-1	1.5VL	44	64	38	76	4	50.8	4.1	102	394	537	105	22.1	9.7	CRF
D7R-2	1.5VL	44	64	38	76	4	50.8	4.1	102	394	537	105	22.1	9.5	CRF
D8-1	1.5VL	44	64	38	76	4	63.5	6.4	95	467	613	105	37.2	11.2	CRF
D8-2	1.5VL	44	64	38	76	4	63.5	6.4	95	467	613	105	37.2	11.9	CRF
D8R-1	1.5VL	44	64	38	76	4	63.5	6.4	102	477	608	105	22.1	9.6	CRF
D8R-2	1.5VL	44	64	38	76	4	63.5	6.4	102	477	608	105	22.1	10.1	CRF
D9-1	1.5VL	44	64	38	76	4	50.8	4.1	95	415	550	99	35.2	8.5	CRF
D9-2	1.5VL	44	64	38	76	4	50.8	4.1	95	415	550	99	35.2	10.1	CRF
D9R-1	1.5VL	44	64	38	76	4	50.8	4.1	102	394	537	99	21.4	8.4	CRF
D9R-2	1.5VL	44	64	38	76	4	50.8	4.1	102	394	537	99	21.4	8.0	CRF
D10-1	1.5VL	44	64	38	76	4	63.5	6.4	95	467	613	99	35.2	10.2	CRF
D10-2	1.5VL	44	64	38	76	4	63.5	6.4	95	467	613	99	35.2	11.2	CRF
D11-1	1.5VL	44	64	38	76	6	50.8	4.1	95	415	550	105	35.2	7.1	CRF
D11-2	1.5VL	44	64	38	76	6	50.8	4.1	95	415	550	105	35.2	7.3	CRF
D12-1	1.5VL	44	64	38	76	6	63.5	6.4	95	467	613	105	35.2	7.3	CRF
D12-2	1.5VL	44	64	38	76	6	63.5	6.4	95	467	613	105	35.2	8.6	CRF
D12R-1	1.5VL	44	64	38	76	6	63.5	6.4	102	477	608	105	22.1	7.3	CRF
D12R-2	1.5VL	44	64	38	76	6	63.5	6.4	102	477	608	105	22.1	7.5	CRF
D13-1	1.5VL	44	64	38	76	1	50.8	6.4	89	456	609	99	24.8	17.3	SS
D13-2	1.5VL	44	64	38	76	1	50.8	6.4	89	456	609	99	24.8	16.9	SS
E1-1	2VL	127	178	51	102	4	31.8	2.8	108	383	530	216	51.0	15.7	SS/SP
E1-2	2VL	127	178	51	102	4	31.8	2.8	108	383	530	216	51.0	18.1	SS/SP
E1R-1	2VL	127	178	51	102	4	31.8	2.8	108	383	530	216	32.4	17.6	SS/SP
E1R-2	2VL	127	178	51	102	4	31.8	2.8	108	383	530	216	32.4	17.3	SS/SP
E2-1	2VL	127	178	51	102	4	50.8	4.7	108	427	590	216	49.6	26.7	SS
E2-2	2VL	127	178	51	102	4	50.8	4.7	108	427	590	216	49.6	27.5	SS
E2R-1	2VL	127	178	51	102	4	50.8	4.7	108	427	590	216	34.5	25.9	SS
E2R-2	2VL	127	178	51	102	4	50.8	4.7	108	427	590	216	34.5	24.9	SS
E3-1	2VL	127	178	51	102	4	50.8	6.4	108	376	534	216	49.6	18.5	SS
E3-2	2VL	127	178	51	102	4	50.8	6.4	108	376	534	216	49.6	21.6	SS
E3R-1	2VL	127	178	51	102	4	50.8	6.4	108	376	534	216	34.5	18.5	SS
E3R-2	2VL	127	178	51	102	4	50.8	6.4	108	376	534	216	34.5	23.3	SS
E3R-3	2VL	127	178	51	102	4	50.8	6.4	108	376	534	216	34.5	22.5	SS
E4-1	2VL	127	178	51	102	4	50.8	4.1	108	394	537	216	34.5	19.1	CRF
E4-2	2VL	127	178	51	102	4	50.8	4.1	108	394	537	216	34.5	16.9	CRF
E5-1	2VL	127	178	51	102	4	50.8	6.4	108	376	534	216	33.1	15.6	CRF
E5-2	2VL	127	178	51	102	4	50.8	6.4	108	376	534	216	33.1	15.0	CRF
E6-1	2VL	127	178	51	102	12	50.8	4.1	114	394	537	223	33.8	12.3	CRF
E6-2	2VL	127	178	51	102	12	50.8	4.1	114	394	537	223	33.8	12.5	CRF
E7-1	2VL	127	178	51	102	12	50.8	6.4	114	376	534	223	26.2	11.7	CRF/SS
E7-2	2VL	127	178	51	102	12	50.8	6.4	114	376	534	223	26.2	12.3	CRF/SS
E8-1	2VL	127	178	51	89	4	50.8	4.7	102	386	521	201	23.4	21.4	CRF/SS
E8-2	2VL	127	178	51	89	4	50.8	4.7	102	386	521	201	23.4	23.0	CRF/SS
E9-1	2VL	127	178	51	89	4	76.2	8.0	102	425	603	201	23.4	15.3	CRF/SS
E9-2	2VL	127	178	51	89	4	76.2	8.0	102	425	603	201	23.4	15.3	CRF/SS
E10-1	2VL	127	178	51	89	6	50.8	6.4	102	400	579	203	23.4	12.7	CRF/SS
E10-2	2VL	127	178	51	89	6	50.8	6.4	102	400	579	203	23.4	14.0	CRF/SS
E11-1	2VL	127	178	51	89	6	76.2	8.0	102	424	602	203	23.4	14.1	CRF/SS
E11-2	2VL	127	178	51	89	6	76.2	8.0	102	424	602	203	23.4	13.3	CRF/SS
F1-1	none	n/a	n/a	n/a	51	n/a	50.8	4.1	64	394	537	n/a	26.2	30.2	SS
F1-2	none	n/a	n/a	n/a	51	n/a	50.8	4.1	64	394	537	n/a	26.2	28.9	SS
F2-1	none	n/a	n/a	n/a	51	n/a	50.8	6.4	64	376	534	n/a	25.5	33.8	SS
F2-2	none	n/a	n/a	n/a	51	n/a	50.8	6.4	64	376	534	n/a	25.5	32.4	SS
F3-1	none	n/a	n/a	n/a	64	n/a	63.5	5.4	76	374	530	n/a	26.2	31.2	SS
F3-2	none	n/a	n/a	n/a	64	n/a	63.5	5.4	76	374	530	n/a	26.2	27.6	SS
F4-1	none	n/a	n/a	n/a	64	n/a	76.2	8.0	76	418	592	n/a	35.2	26.8	SS
F4-2	none	n/a	n/a	n/a	64	n/a	76.2	8.0	76	418	592	n/a	35.2	25.0	SS
F6-1	none	n/a	n/a	n/a	76	n/a	88.9	9.5	89	351	530	n/a	38.6	27.4	SS
F6-2	none	n/a	n/a	n/a	76	n/a	88.9	9.5	89	351	530	n/a	38.6	26.8	SS

Table AH.1(cont'd) Summary of Push-out Test Parameters and Results

Test No.	Deck	w_{r1} (mm)	w_{r2} (mm)	h_r (mm)	H_s (mm)	N	w_{tc} (mm)	t_{tc} (mm)	t_s (mm)	F_{ytc} (MPa)	F_{utc} (MPa)	l_s (mm)	f'_c (MPa)	R_t (kN)	Failure[c]
H1-1	3VL	121	184	76	114	4	38.1	3.9	127	402	536	206	22.8	14.9	CRF
H1-2	3VL	121	184	76	114	4	38.1	3.9	127	402	536	206	22.8	13.9	CRF
H2-1	3VL	121	184	76	114	4	50.8	4.7	127	386	521	206	22.8	17.3	CRF
H2-2	3VL	121	184	76	114	4	50.8	4.7	127	386	521	206	22.8	14.4	CRF
H2-3	3VL	121	184	76	114	4	50.8	4.7	127	386	521	206	22.8	14.0	CRF
H3-1	3VL	121	184	76	114	4	50.8	6.4	127	420	590	206	22.8	16.2	CRF
H3-2	3VL	121	184	76	114	4	50.8	6.4	127	420	590	206	22.8	12.7	CRF
H3-3	3VL	121	184	76	114	4	50.8	6.4	127	420	590	206	22.8	15.5	CRF
H4-1	3VL	121	184	76	114	6	50.8	6.4	127	420	590	207	22.8	9.6	CRF
H4-2	3VL	121	184	76	114	6	50.8	6.4	127	420	590	207	22.8	11.3	CRF
H4-3	3VL	121	184	76	114	6	50.8	6.4	127	420	590	207	22.8	11.2	CRF
H5-1	3VL	121	184	76	114	6	76.2	8.0	127	424	602	207	30.3	12.2	CRF
H5-2	3VL	121	184	76	114	6	76.2	8.0	127	424	602	207	30.3	11.6	CRF
H6-1	3VL	121	184	76	114	8	76.2	8.0	127	424	602	209	30.3	12.4	CRF
H6-2	3VL	121	184	76	114	8	76.2	8.0	127	424	602	209	30.3	10.1	CRF
H6-3	3VL	121	184	76	114	8	76.2	8.0	127	424	602	209	30.3	10.1	CRF
H7-1	3VL	121	184	76	114	8	76.2	9.5	127	351[b]	530[b]	209	30.3	11.3	CRF
H7-2	3VL	121	184	76	114	8	76.2	9.5	127	351[b]	530[b]	209	30.3	11.7	CRF
H8-1	3VL	121	184	76	127	8	76.2	8.0	127	424	602	226	30.3	12.7	CRF
H8-2	3VL	121	184	76	127	8	76.2	8.0	127	424	602	226	30.3	13.5	CRF

[a] One slab is attached to 4.1 mm thick angle; failure occurred at the opposite slab, attached to a 6.4 mm angle.

[b] Estimated.

[c] SP = screw pullout, SS = screw shear, CRF = concrete rib failure;